Title: Functional characterization of TANGLED1 interaction with PHRAGMOPLAST ORIENTING KINESIN1 during mitosis in Arabidopsis

Running title: Key motifs mediate TAN1 function and localization

Alison M. Mills[1], Victoria H. Morris[2,3], Carolyn G Rasmussen[1,2,*]

[1]Graduate Group in Biochemistry and Molecular Biology
[2]Department of Botany and Plant Sciences, Center for Plant Cell Biology, Institute of Integrative Genome Biology, University of California, Riverside.
[3]Current address: Brandeis University, Waltham, MA

[*]Correspondence to Carolyn Rasmussen: carolyn.rasmussen@ucr.edu

ORCID CGR 0000-0002-4354-6295
ORCID AMM 0000-0002-7391-1409
ORCID VHM 0000-0003-4881-6343

Keywords: mitosis, cytokinesis, TANGLED1, AIR9, phragmoplast, POK1, division plane orientation, Arabidopsis

One sentence summary: Specific amino acids within TAN1 are required for its correct localization and function partially through interaction with POK1; both TAN1 and AIR9 mediate POK1 division site localization.

Abstract:

Cell division requires spatial coordination to properly position the division plane. How division plane positioning contributes to plant growth remains unknown. Two unrelated microtubule binding proteins, TANGLED1 (TAN1) and AUXIN-INDUCED-IN-ROOT-CULTURES9 (AIR9), are together required for normal Arabidopsis growth and division. *tan1 air9* double mutants have synthetic growth and division plane orientation defects while single mutants lack obvious defects. We show that the first 132 amino acids of TAN1 ($TAN1_{1-132}$) rescue the *tan1 air9* double mutant and localize to the division site during telophase. Loss of both rescue and division-site localization occurred when interaction between TAN1 and PHRAGMOPLAST ORIENTING KINESIN1 (POK1) was disrupted by replacing six amino acid residues with alanines in $TAN1_{1-132}$. However, full-length TAN1 with the same alanine substitutions significantly rescued the *tan1 air9* double mutant and remained at the division site throughout mitosis, although its accumulation was reduced and phragmoplast positioning defects occurred. POK1 often fails to accumulate at the division site in *tan1 air9* mutants, suggesting that both TAN1 and AIR9 stabilize POK1 there. Finally, a mitosis specific promoter driving *TAN1* rescued the *tan1 air9* double mutant phenotypes indicating that defects seen in the root differentiation zone reflect the loss of mitotic-specific TAN1 activity.

Introduction

Division plane orientation is important for many aspects of plant, microbial, and animal development, particularly growth and patterning. Division plane orientation is especially relevant for plant cells which are confined by cell walls, and unable to migrate (Rasmussen and Bellinger, 2018; Livanos and Müller, 2019; Facette et al., 2018; Wu et al., 2018). Positioning and construction of the new cell wall (cell plate) during cytokinesis involves two microtubule- and microfilament-rich cytoskeletal structures, the preprophase band (PPB) and the phragmoplast (Smertenko et al., 2017). The PPB is a ring of microtubules, microfilaments, and proteins that forms at the cell cortex just beneath the plasma membrane during G2: this region is defined as the cortical division zone (Van Damme, 2009; Smertenko et al., 2017; Li et al., 2015). The cortical division zone is characterized by active endocytosis mediated by TPLATE-clathrin coated vesicles that may deplete actin and the actin-binding kinesin like-protein KCA1/KAC1 (Vanstraelen et al., 2004; Suetsugu et al., 2010; Karahara et al., 2009; Kojo et al., 2013; Panteris, 2008; Hoshino et al., 2003). The PPB disassembles after nuclear envelope breakdown to form the metaphase spindle, an antiparallel microtubule array (Dixit and Cyr, 2002). After the chromosomes are separated, the phragmoplast is constructed from spindle remnants to form an antiparallel array of microtubules with their dynamic plus ends directed towards the middle of the cell (Lee and Liu, 2019). The phragmoplast microtubules are tracks for the movement of vesicles containing cell wall materials towards the forming cell plate (McMichael and Bednarek, 2013; Müller and Jürgens, 2016). The phragmoplast expands by nucleation of new microtubules on pre-existing microtubules (Murata et al., 2013; Smertenko et al., 2018) and is partially dependent on the mitotic microtubule binding protein ENDOSPERM DEFECTIVE1 and the AUGMIN complex to recruit gamma tubulin to microtubules (Lee et al., 2017; Nakaoka et al., 2012). Finally, the phragmoplast reaches the cell cortex and the cell plate and associated membranes fuse with the mother cell membranes at the cell plate fusion site previously specified by the PPB (van Oostende-Triplet et al., 2017).

TANGLED1 (TAN1, AT3G05330) was the first identified protein that localizes to the plant division site throughout mitosis and cytokinesis (Walker et al., 2007). In maize, the *tan1* mutant has defects in division plane orientation caused by phragmoplast guidance defects (Cleary and Smith, 1998; Martinez et al., 2017). TAN1 bundles and crosslinks microtubules in vitro (Martinez et al., 2020). In vivo, TAN1 promotes microtubule pausing at the division site (Bellinger et al., 2021). Critically, TAN1, together with other division site localized proteins, organizes an array of cell cortex localized microtubules that is independent from the phragmoplast. These cortical-telophase microtubules accumulate at the cell cortex during telophase and are subsequently incorporated into the phragmoplast to direct its movement towards the division site (Bellinger et al., 2021). Other important division site localized proteins were identified through their interaction with TAN1, such as the kinesin-12 protein PHRAGMOPLAST ORIENTING KINESIN1 (POK1) and POK2 (Müller et al., 2006), (Lipka et al., 2014). Together, POK1 and POK2 are required to guide the phragmoplast to the division site (Herrmann et al., 2018; Müller et al., 2006). Similar to other kinesin-12 proteins, PHRAGMOPLAST ASSOCIATED KINESIN RELATED PROTEIN (PAKRP1) and PAKRPL1 (Lee et al., 2007; Pan et al., 2004), POK2

localizes to the phragmoplast midline during telophase and plays a role in phragmoplast expansion (Herrmann et al., 2018).

In Arabidopsis, *tan1* mutants have very minor phenotypes (Walker et al., 2007). However, combination of *tan1* with *auxin-induced-in-root-cultures9* (*air9),* a mutant with no obvious defects (Buschmann et al., 2015), resulted in a synthetic phenotype (Mir et al., 2018). TAN1 and AIR9 are unrelated microtubule-binding proteins that both localize to the division site (Walker et al., 2007; Buschmann et al., 2006). The *tan1 air9* double mutant plants were short with twisted roots, and had significant defects in phragmoplast guidance (Mir et al., 2018). When full length *TAN1* was transformed into the *tan1 air9* double mutant, *TAN1* rescued the phenotype so that plants looked similar to wild-type, but when *TAN1* missing the first ~130 amino acids was transformed into the *tan1 air9* double mutant, no rescue was observed. This suggests that this part of the TAN1 protein is critical for function in root growth and division plane positioning.

We hypothesized that TAN1 had a role in organizing interphase microtubules, because defects occured in *tan1 air9* double mutant cells undergoing expansion or differentiation in addition to defects in division plane positioning. The *tan1 air9* double mutant had aberrant cell file rotation in the root differentiation zone. In addition, *tan1 air9* double mutants not only had minor defects in interphase microtubule organization, but root growth defects were also enhanced by the microtubule depolymerizing drug propyzamide (Mir et al., 2018). Together, this suggested that cell file rotation defects were likely caused by alterations in interphase microtubule organization. Cell file rotation phenotypes are often caused by mutations in microtubule associated proteins or tubulin and therefore are thought to alter the organization or stability of the interphase cortical microtubule array (Buschmann and Borchers, 2020; Ishida et al., 2007; Abe et al., 2004; Sedbrook et al., 2004; Nakajima et al., 2004; Shoji et al., 2004; Buschmann et al., 2004; Hashimoto, 2015; Sakai et al., 2008). For example, in several *alpha-tubulin* mutants, cell file rotation occurred both in hypocotyls and root differentiation zones where cell division does not occur and in isolated cultured mutant cells (Abe et al., 2004; Ishida et al., 2007; Thitamadee et al., 2002; Buschmann et al., 2009). This indicated that defects in organ twisting were likely independent of cell division defects. However, while many mutants with cell file rotation defects are likely due to alterations to interphase cortical microtubule organization, several examples point towards more specific defects during cell division in Arabidopsis roots (Wasteneys and Collings, 2009). Mutants with defects in division plane orientation within the quiescent center (QC), *tornado1* and *tornado2* and interacting partners *wih1* and *wih2,* have twisted roots (Cnops et al., 2000; Lieber et al., 2011), while double mutants in two related receptor-like kinases, *irk pxc2,* have defects in division plane orientation in the QC and endodermis and abnormal root skewing (Goff and Van Norman, 2021).

Here, we show that mitotic specific functions of TAN1 rescue the *tan1 air9* double mutant, and that interactions between TAN1, AIR9 and POK1 are important for division plane orientation, perhaps due to their stabilization or recruitment to the division site during telophase through protein-protein interactions.

Results:

Amino acids 1-132 of TAN1 Rescue the *tan1 air9* Double Mutant

TAN1 missing the first 126 amino acids failed to rescue the *tan1 air9* double mutant, suggesting that this region of the protein is critical for TAN1 function (Mir et al., 2018). To test the function of this part of the protein in vivo, the *TAN1* coding sequence encoding the first 132 amino acids was fused to Yellow Fluorescent Protein (YFP, $TAN1_{1-132}$-YFP) driven by the cauliflower mosaic 35S promoter and was then transformed into the *tan1 air9* double mutant. The progeny of several independent transformed lines with *p35S:*$TAN1_{1-132}$*-YFP* rescued the *tan1 air9* double mutant, as described in more detail below. Overall root patterning of *tan1 air9* double mutants expressing either *p35S:*$TAN1_{1-132}$*-YFP* or full length *p35S:TAN1-YFP* was restored, while untransformed *tan1 air9* double mutants roots had misoriented divisions (Figure 1A**,** Supplementary Figure 1). Cell file rotation, which skews left and has large variance in the *tan1 air9* double mutant (Figure 1B, Figure 1C) was significantly rescued in both *p35S:*$TAN1_{1-132}$*-YFP* and *p35S:TAN1-YFP tan1 air9* lines (n = 37 and 41 plants respectively, compared to the untransformed *tan1 air9* control (Levene's test, P-value < 0.0001). Root length at 8 days after stratification was also restored (Figure 1D). Interestingly, although $TAN1_{1-132}$-YFP rarely co-localizes with PPBs in wild-type plants (Rasmussen et al., 2011) or in *tan1 air9* double mutants (Figure 3A, 10 % n = 9/89), PPB angles of *p35S:*$TAN1_{1-132}$*-YFP* and *p35S:TAN1-YFP* in *tan1 air9* double mutants had significantly less variance compared to the untransformed control (Figure 1E). Phragmoplast positioning defects of the *tan1 air9* double mutant were also significantly rescued by *p35S:*$TAN1_{1-132}$*-YFP*. Therefore, *p35S:*$TAN1_{1-132}$*-YFP* rescued the phenotypes of the double mutant similar to full-length *p35S:TAN1-YFP.* This indicates that most functions that affect noticeable phenotypes are encoded by the first section of the *TAN1* gene.

Disrupting TAN1-POK1 interaction reduces $TAN1_{1-132}$-YFP localization to the division site and abrogates *tan1 air9* rescue

Since *p35S:*$TAN1_{1-132}$*-YFP* effectively rescued the *tan1 air9* double mutant, we focused on further understanding how TAN1 functioned by disrupting its ability to interact with the kinesin POK1. POK1 interacts specifically with $TAN1_{1-132}$ via the yeast-two hybrid system (Rasmussen et al., 2011), so alanine scanning mutagenesis was used to systematically replace six amino acids with six alanines tiled across $TAN1_{1-132}$ (described in materials and methods). These constructs were tested for interaction with POK1 using the yeast two hybrid system. Seven of seventeen constructs tested lost interaction with POK1, suggesting that these amino acids were important for POK1-TAN1 interaction (Supplementary Figure 2). One of these, $TAN1_{1-132}$ with alanine substitutions replacing amino acids 28-33 INKVDK with six alanines $(TAN1(28\text{-}33A)_{1-132}$), was then cloned into a plant transformation vector to generate *p35S:*$TAN1(28\text{-}33A)_{1-132}$ *-YFP*. *p35S:*$TAN1(28\text{-}33A)_{1-132}$ *-YFP* was transformed into the *tan1 air9* double mutant. Our hypothesis was that POK1 interaction with TAN1 would be critical for TAN1 function and disruption of the interaction would block *p35S:*$TAN1_{1-132}$*-YFP* rescue of the *tan1 air9* double mutant. The *p35S:*$TAN1(28\text{-}33A)_{1-132}$ *-YFP* construct partially rescued the *tan1 air9* double mutant (Figure 2). *p35S:*$TAN1(28\text{-}33A)_{1-132}$ *-YFP* in the *tan1 air9* double mutant did not rescue cell file rotation defects (Figure 2B, D) or phragmoplast angle defects (Figure 2F). However, overall plant growth (Figure 2C) and root length (Figure 2E) showed intermediate rescue

compared to unaltered *p35S:TAN1$_{1-132}$-YFP* in the *tan1 air9* double mutant. PPB angles in *tan1 air9* double mutants expressing either *p35S:TAN1(28-33A)$_{1-132}$ -YFP* or *p35S:TAN1$_{1-132}$-YFP* were similar, suggesting that TAN1-POK1 interaction is not required for PPB placement (Figure 2F). These results suggest that the first 132 amino acids of TAN1 perform several vital functions, many of which are contingent or partially contingent on interaction with POK1. Partial rescue indicates that TAN1$_{1-132}$ mediates activities critical for growth independent of POK1, possibly through yet unknown protein-protein interactions.

Localization of TAN1(28-33A)$_{1-132}$ -YFP to the division site during telophase was significantly reduced compared to unaltered TAN1$_{1-132}$-YFP, which localized to the division site during telophase 100% of the time (n = 58/58, Figures 3E, (Rasmussen et al., 2011)). TAN1(28-33A)$_{1-132}$ -YFP showed no obvious division site localization 68% of the time (n = 15/22, Figure 3I) or faint division site accumulation in 32% of telophase cells (n = 7/22 Figure 3J). When the fluorescence intensity of TAN1(28-33A)$_{1-132}$ -YFP at the division site during telophase was compared to the cytosolic fluorescence intensity in the same cell, the median ratio was ~1.1 indicating little preferential accumulation of TAN1(28-33A)$_{1-132}$ -YFP at the division site (Figure 3K). In contrast, the median ratio of unaltered TAN1$_{1-132}$-YFP at the division site was ~1.8 compared to cytosolic fluorescence, indicating its preferential accumulation at the division site. This suggests that POK1 interaction with TAN1 is disrupted by replacing amino acids 28-33 in TAN1 with alanines, and that preferential localization of TAN1$_{1-132}$-YFP to the division site during telophase is dependent on this interaction with POK1.

Direct POK1 and TAN1 interaction is critical to recruit TAN1$_{1-132}$ to the division site during telophase and may additionally be required for phragmoplast guidance to the division site. Next, we assessed whether TAN1-POK1 interaction would mediate division site localization and rescue with full length TAN1 by generating the same alanine substitutions, then transforming full-length *p35S:YFP-TAN1(28-33A)* into *tan1 air9* double mutants. In contrast to the modest partial rescue provided by *p35S:TAN1(28-33A)$_{1-132}$ -YFP*, full-length *p35S:YFP-TAN1(28-33A)* significantly rescued the *tan1 air9* double mutant. (Figure 4, Supplementary Figure 3). Cell file rotation (Figure 4C), root length (Figure 4D) and PPB angles (Figure 4E) were similar to the *air9* single mutant, while phragmoplast angles were partially rescued. Similar to TAN1-YFP (Figure 5A, B), YFP-TAN1(28-33A) localized to the division site in preprophase, prophase and telophase (Figure 5C, 5D). YFP-TAN1(28-33A) fluorescence intensity levels were measured (n = 11 plants). During prophase, YFP-TAN1(28-33A) fluorescence intensity at the division site compared to the cytosol was similar to TAN1-YFP fluorescence intensity ratios (n = 13 plants). In contrast, YFP-TAN1(28-33A) fluorescence intensity ratios were reduced to ~1.6 compared with unaltered TAN1-YFP (~2.1) indicating that YFP-TAN1(28-33A) accumulated less at the division site during telophase (Figure 5E). Together, these data indicate that TAN1 is recruited to the division site during prophase without interaction with POK1. Further, POK1 is important but not essential for TAN1 localization during telophase if TAN1 is already at the division site. Defects in phragmoplast positioning may be due specifically to the disruption of TAN1-POK1 interaction, or due to the lower accumulation of TAN1 at the division site that would normally be mediated by POK1 during telophase.

We examined POK1 localization in the *tan1 air9* double mutants to determine whether TAN1 and AIR9 were essential for POK1 localization. Our hypothesis was that POK1 localization would not be contingent on *TAN1* or *AIR9*, and therefore unaltered in the *tan1 air9* double mutant. In wild-type cells, YFP-POK1 localized as expected to the division site during preprophase/prophase (n = 40 cells, Figure 6A) and during telophase/cytokinesis (Figure 6B, n = 76 cells, 17 plants), similar to previous studies (Lipka et al., 2014). Rarely, YFP-POK1 additionally accumulated in the phragmoplast midline (4%, n = 3/76, Figure 6C). In the *tan1 air9* double mutant, YFP-POK1 localized to the division site as expected during preprophase/prophase (n = 17 cells, 9 plants, Figure 6D). Surprisingly, YFP-POK1 localization was no longer at the division site in over half the telophase cells but instead accumulated only at the phragmoplast midline (61%, n = 14/23 cells, Figure 6F). The rest of the telophase cells showed normal division site localization (39%, n = 9/23 cells, Figure 6E). This result suggests that TAN1 and/or AIR9 stabilize or recruit POK1 to the division site during telophase. To identify whether TAN1 or AIR9 worked individually or together to mediate POK1 division site localization, we analyzed YFP-POK1 localization in single *tan1* and *air9* mutants. YFP-POK1 accumulated during preprophase/prophase in *tan1* mutants (Figure 6G, n = 10 cells, 6 plants) and *air9* mutants (Figure 6J, n = 12 cells, 6 plants). In addition, YFP-POK1 also accumulated at the division site during telophase and cytokinesis in both *tan1* and *air9* mutants. In *tan1* single mutants, YFP-POK1 localized only to the division site in 74% of cells (Figure 6H, n = 20/27), while it localized both to the division site and the phragmoplast midline in 26% of cells (Figure 6I, n = 7/27). In 83% of *air9* single mutant cells YFP-POK1 localized solely to the division site (Figure 6K, n = 15/18), while 17% localized to both the division site and the phragmoplast midline (Figure 6L, n = 3/18). Neither *tan1* nor *air9* single mutants had YFP-POK1 localization solely to the phragmoplast midline (n = 27 and 18 telophase cells respectively). During telophase, YFP-POK1 localized to the division site in either *tan1* or *air9* single mutants but not in the *tan1 air9* double mutant, indicating that TAN1 and AIR9 both stabilize YFP-POK1 at the division site. Individually either TAN1 or AIR9 is sufficient to recruit or stabilize POK1 at the division site during telophase.

Mitotic TAN1 expression rescues "interphase" cell file rotation defects

Despite significant rescue of the cell file rotation defect, neither full length *TAN1-YFP* nor *TAN1*$_{1-132}$*-YFP* driven by the 35S promoter in the *tan1 air9* double mutant restored cell file rotation to single mutant *air9* levels (e.g. Figure 4 C). This suggested that the *35S* promoter driving TAN1-YFP might partially disrupt its ability to rescue the *tan1 air9* double mutant, particularly in differentiated cells. Whether patchy expression in dividing cells or aberrant overexpression in non-dividing cells disrupted the ability of *p35S:TAN1-YFP* to rescue the *tan1 air9* double mutant was unclear. Further, it was unclear whether cell file rotation rescue was primarily dependent on interphase or mitotic TAN1 function. Using the mitosis specific promoter from the syntaxin *KNOLLE* (Völker et al., 2001), we drove expression of full-length *TAN1-YFP* (*pKN:TAN1-YFP*) in *tan1 air9* double mutants. Our hypothesis was that division plane defects would be rescued, but "interphase" cell file rotation defects would still exist in the *pKN:TAN1-YFP tan1 air9* lines. Not surprisingly, *pKN:TAN1-YFP* was expressed strongly in the dividing zone of root tips, localizing as expected with the PPB and at the division site during metaphase and telophase (Figure 7B, Supplementary Figure 4). Indeed, TAN1-YFP driven by the *KNOLLE* promoter had

much higher accumulation in the meristematic zone than TAN1-YFP driven by the *35S* promoter (Figure 7G). TAN1-YFP fluorescence driven by the *KNOLLE* promoter was not observed above background levels in either the elongation zone (Figure 7D) or the differentiation zone (Figure 7F). To our surprise, *pKN:TAN1-YFP* rescued both division defects and cell file rotation defects in *tan1 air9* double mutants as well as *p35S:TAN1-YFP* (Figure 8, other independent transgenic lines in Supplementary Figure 5). These data indicate that lack of mitotic TAN1, rather than lack of interphase TAN1 drives cell file rotation defects within the *tan1 air9* double mutant.

Discussion

The first 132 amino acids of TAN1, $TAN1_{1-132}$, which rarely localize to the division site during prophase or metaphase, accumulate at the division site during telophase and rescue the *tan1 air9* double mutant. Both rescue and localization of $TAN1_{1-132}$ -YFP to the division site are partially dependent on interaction with the kinesin POK1. Disruption of the TAN1-POK1 interaction, by replacing 6 amino acids (28-33) with alanines, significantly hampered the ability of *p35S:*$TAN1_{1-132}$*-YFP(28-33A)* to rescue the *tan1 air9* double mutant. However, when the full-length *p35S:YFP-TAN1(28-33A)* was transformed into the *tan1 air9* double mutant, it fully rescued the root growth and twisting defects, and partially rescued PPB and phragmoplast positioning defects. YFP-TAN1(28-33A) also localized to the division site throughout mitosis and cytokinesis, even though interactions with POK1 were interrupted. However, YFP-TAN1(28-33A) accumulated at the division site less during telophase than during prophase and *p35S:YFP-TAN1(28-33A)* had more phragmoplast positioning defects than *p35S:TAN1-YFP* in the *tan1 air9* double mutant. Whether phragmoplast positioning defects were due to reduced TAN1 accumulation at the division site or due to lack of TAN1-POK1 interaction is unknown. Since POK1 localization to the division site during telophase occurs less frequently in the *tan1 air9* double mutant, it is plausible to assume that POK1 division site localization may be similarly interrupted by disruption of the POK1-TAN1 interaction when the only source of TAN1 or AIR9 is YFP-TAN1(28-33A) in the *tan1 air9* double mutant. However, the significant rescue of most double mutant phenotypes when expressing *p35S:YFP-TAN1(28-33A)* highlight the redundancy built into TAN1 localization to the division site, and ability to function *in planta*. Previously, a cyclin-B destruction box was fused to maize *TAN1* to promote ubiquitin-mediated degradation during anaphase. Even a 10-fold reduction in TAN1-YFP accumulation at the division site during telophase did not affect division plane positioning. Therefore, very little TAN1 protein is required during telophase to achieve proper phragmoplast positioning in maize (Martinez et al., 2017). Additionally, our data show that TAN1 is essential during telophase, but that POK1-independent mechanisms promote its colocalization with the PPB, and to a lesser extent division site localization during telophase. It is possible that TAN1 is recruited to the PPB by its direct interaction with microtubules (Martinez et al., 2020), although additional mechanisms cannot be ruled out.

Intriguingly, POK1 localization during telophase was also dependent on TAN1 and AIR9. POK1 often failed to localize to the division site during telophase in *tan1 air9* double mutants, but instead accumulated at the phragmoplast midline. Together, this suggests that TAN1, AIR9 and POK1 are mutually dependent on each other for localization to the division site during telophase. POK1 accumulation at the phragmoplast midline was rarely seen in wild-type cells (Figure 6, (Lipka et al., 2014)). A closely related kinesin, POK2, showed striking dual localization to both the phragmoplast midline and the division site. Localization of POK2 to the phragmoplast midline required the N-terminal motor domain, while the C-terminal region was localized to the division site (Herrmann et al., 2018). Neither of these separate parts of POK2 were capable of rescuing the *pok1 pok2* double mutant division plane defects. We speculate that the default location of both POK1 and POK2, based on likely or confirmed plus-end directed motor activity (Chugh et al., 2018), is at microtubule plus-ends that accumulate at the

phragmoplast midline. Interactions with other division site localized proteins, such as TAN1 and AIR9, may stabilize or recruit them at the division site.

Analysis of the mitosis-specific expression of TAN1 driven by the *KNOLLE* promoter suggests that division plane orientation and/or additional mitotic-specific functions of TAN1 are sufficient to rescue the defects of the *tan1 air9* double mutant. This result is consistent with previous data showing that *TAN1* driven by its own promoter is not observed in differentiation zone root cells (Mir et al., 2018), and that *TAN1* expression is restricted to tissues with active division (Walker et al., 2007). *TAN1* expression is contingent on two related MYB (myeloblastosis) transcription factors that promote mitosis specific gene expression (Yang et al., 2021; Haga et al., 2011). The MYB transcription factors in turn activate a GRAS-type (GIBBERELLIC-ACID INSENSITIVE (GAI), REPRESSOR of GAI (RGA) and SCARECROW (SCR)- type) transcription factor SCL28 during G2/M, which by activating gene expression is both important for mitotic progression and for proper division plane positioning (Goldy et al., 2021). It is likely that *TAN1* and other genes important for division plane positioning are partially or completely dependent on these transcription factors.

Together, data presented here specify the most likely time, telophase, and location, at the division site, required for TAN1 to perform essential functions in division plane positioning, with indirect functions in root growth and twisting.

Materials and methods

Growth conditions, genotyping mutants, and root length measurements

Arabidopsis seedlings were grown on ½ strength Murashige and Skoog (MS) media (MP Biomedicals; Murashige and Skoog, 1962) containing 0.5 g/L MES (Fisher Scientific, pH 5.7, and 0.8% agar (Fisher Scientific). Seeds sown on plates were first stratified in the dark at 4°-8°C for 2 to 5 days then grown vertically in a growth chamber (Percival) with 16/8-h light/dark cycles and temperature set to 22°C. For root length experiments, *tan1 air9* transgenic T3 lines expressing *p35S:TAN1-YFP, 35S:TAN1*$_{1\text{-}132}$*-YFP, pKN:TAN1-YFP,* or *35S:YFP-TAN1(28-33A)*$_{1\text{-}132}$ were grown vertically, the plates were scanned (Epson) and root lengths were measured using FIJI (ImageJ, http:/ /fiji.sc/) after 8 days. Root lengths were then plotted using Prism (GraphPad). Statistical analysis of root length was performed with Prism (GraphPad) using t test with Welch's correction. After plates were scanned, seedlings were screened by microscopy to identify seedlings expressing YFP translational fusion transgenes and CFP-TUBULIN, if present in the transgenic line.

TAN1 transgenes were analyzed in *csh-tan* (*TAN1,* AT3G05330) *air9-31* (*AIR9*, AT2G34680) double mutants in *Landsberg erecta (Ler)*. The *pPOK1:YFP-POK1* transgene in Columbia, (a kind gift from Sabine Müller, (Lipka et al., 2014)) was crossed into the *tan-mad* and *air9-5* Columbia/Wassilewskija double mutant previously described (Mir et al., 2018). *tan-mad* and *air9-5* mutants were genotyped with primers ATRP and ATLP (to identify TAN wild type), JL202 and ATRP (to identify T-DNA insertion in *TAN1*), AIR9-5RP and AIR9-5LP (to identify wild-type *AIR9*), and LBb1.3 and AIR9RP (to identify T-DNA insertion in *AIR9*) and by observation of the *tan1 air9* double mutant phenotype (Supplementary Table 1).

365
366 Generation of Transgenic Lines
367 *Agrobacterium tumefaciens*-mediated floral dip transformation was used as described (Clough
368 and Bent, 1999). *csh-tan air9-31* double mutants were used for all floral dip transformations.
369 Transgenic plants were selected on 15 µg/mL glufosinate (Finale; Bayer) and screened by
370 microscopy before being transferred to soil and selfed. *CFP-TUBULIN* was crossed into
371 *pKN:TAN1-YFP* and *35S:TAN1(28-33A)$_{1-132}$ -YFP tan1 air9* plants using *tan1 air9 CFP-*
372 *TUBULIN* plants (Mir et al., 2018) and progeny were subsequently screened by microscopy for
373 CFP and YFP signal. *csh-tan1 air9-31* double mutants were confirmed by genotyping with
374 primers ATLP and AtTAN 733-CDS Rw (to identify TAN1 wild type), AtTAN 733-CDS Rw and
375 Ds5-4 (to identify T-DNA insertion in *TAN1*), AIR9_cDNA 2230 F and AIR9 gnm7511 R (to
376 identify *AIR9* wild type), and AIR9 gnm7511 R and Ds5-4 (to identify T-DNA insertion in *AIR9*).
377
378 Plasmid Construction
379 *TAN1$_{1-132}$ -YFP* coding sequences were subcloned by EcoRI and BamHI double digestion from
380 the plasmid *pEZRK-LNY-TAN1$_{1-132}$ -YFP* described previously (Rasmussen et al., 2011) into
381 *pEZT-NL* vector (a kind gift from David Ehrhardt, Carnegie Institute, Stanford University) and
382 selected with glufosinate (Finale; Bayer). The CFP-TUBULIN (CFP-TUA6) vector was
383 previously described (Kirik et al., 2007).
384
385 Six amino acid alanine substitutions were generated using overlapping PCR (primers in
386 Supplementary Table 1) beginning at amino acid 10 of TAN1$_{1-132}$. *TAN1$_{1-132}$ -YFP* coding
387 sequence from plasmids described previously was used as the PCR template (Rasmussen et
388 al., 2011). *TAN1(28-33A)$_{1-132}$ -YFP* was subcloned by EcoRI BamHI double digestion into pEZT-
389 NL. To generate *YFP-TAN1(28-33A)*, alanine substitutions were first introduced into G22672
390 (TAN1 cDNA in pENTR223, from the Arabidopsis Biological Resource Center) using
391 overlapping PCR with the same primers to generate *TAN1(28-33A)$_{1-132}$*. Gateway reaction
392 (Fisher Scientific) was then used to subclone *TAN1(28-33A)* into pEarley104 (Earley et al.,
393 2006).
394
395 *pKN:TAN1-YFP* was generated by amplifying 2152 bp of the 5' KNOLLE promoter from
396 Columbia with primers pKN-5'SacI Fw and pKN-5'EcoRI Rw. EcoRI and StuI double digestion
397 was used to introduce the *KNOLLE* promoter into pEZT-NL containing the TAN1 coding
398 sequence. Using primers 35SpKN5' Fw and YFP XhoI Rw to amplify, followed by XhoI and StuI
399 double digestion, *pKN:TAN1-YFP* was cloned into pEGAD (kind gift of Sean Cutler).
400
401 Microscopy
402 An inverted Ti Eclipse (Nikon) with motorized stage (ASI Piezo) and spinning-disk confocal
403 microscope (Yokogawa W1) built by Solamere Technology was used with Micromanager
404 software (micromanager.org). Solid-state lasers (Obis) and emission filters (Chroma
405 Technology) were used. For CFP-TUBULIN excitation 445, emission 480/40 was used; YFP
406 translational fusions excitation 514, emission 540/30; and propidium iodide (PI) and Alexa-568
407 goat anti-mouse antibody excitation 561, emission 620/60 were used. The 20x objective has

0.75 numerical aperture and the 60x objective has 1.2 numerical aperture objective which was used with perfluorocarbon immersion liquid (RIAAA-6788 Cargille).

Measurements of PPB and phragmoplast angles and cell file rotation

8 day-old seedlings were stained with 10 µM PI for 1 minute and then destained in distilled water before imaging by confocal microscopy using a 20x or 60x objective. PPB and phragmoplast angles were measured using FIJI. The angle was measured between the left hand cell wall and the orientation of the PPB or phragmoplast in the root tips of *tan1 air9* double mutants expressing CFP-TUBULIN or immunostained microtubules (described in the next section). Cell file rotation was examined by measuring from the left hand side of the transverse cell wall relative to the long axis of the root in images of the differentiation zone stained with PI. The differentiation zone was identified by the presence of root hairs. Prism (GraphPad) and Excel (Microsoft Office) were used to perform statistical analyses and to plot data. F-test was used to compare normally distributed variances (PPB and phragmoplast angles) and Levene's test was used to compare non-normally distributed variances (cell file angle measurements) in Excel.

Immunostaining

air9, tan1 air9 p35S:TAN1-YFP, tan1 air9, 35S:YFP-TAN1(28-33A), and untransformed *tan1 air9* plants were stratified and then grown vertically on ½ MS plates in a growth chamber at 22°C with a 16/8-h light/dark cycle for 8 days. The seedlings were screened by microscopy for YFP and then fixed and processed for immunofluorescence microscopy using a 1:2000 dilution of monoclonal anti-α-tubulin B-5-1-2 antibody (Life Technologies; 32-2500) followed by 1:2000 dilution of Alexa-568 goat anti-mouse antibody (Thermo Fisher; A-11004) as described previously (Sugimoto et al., 2000).

Yeast two hybrid

Six alanine substitutions were generated using overlapping PCR and TAN1 coding sequence in pEZRK-LNY-$TAN1_{1\text{-}132}$-*YFP* as a template beginning at amino acid 10 of TAN1 and continuing through amino acid 123 according to (Sambrook and Russell, 2001). The substitution constructs were cloned into pAS vector (Fan et al., 1997) using EcoRI BamHI double digestion. pBD-TAN1 (Walker et al., 2007), and pAS-$TAN1_{1\text{-}132}$ *(Rasmussen et al., 2011)* were used as positive controls, while pAD-MUT was used as a negative control for testing interaction with pAD-POK1 (Müller et al., 2006). *pAD-POK1* and *pAS-*$TAN1_{1\text{-}132}$ constructs were co-transformed into yeast strain YRG2 according to manufacturer instructions (Stragene). Positive yeast two-hybrid interaction was determined by the presence of growth on plates cultured at 30°C lacking histidine after 3 days. Plates were then scanned (Epson).

Acknowledgements

Thanks to Andrew Gomez (UCR, supported by USDA-NIFA 2017-38422-27135) for help with yeast-two-hybrid experiments, Prof. Sabine Müller (University of Tübingen) for YFP-POK1 seeds, and Profs. Meng Chen and David Nelson (UCR) for their helpful comments on alanine scanning mutagenesis. Thanks to Prof. Henrik Buschmann (Osnabrück University) for original *tan1 air9* characterization. Thanks to Lindy Allsman, Stephanie Martinez, and Aimee Uyehara

452 (UCR) for helpful comments on the manuscript. NSF-CAREER #1942734 and#1716972, USDA-
453 NIFA-CA-R-BPS-5108-H are gratefully acknowledged for funding.
454

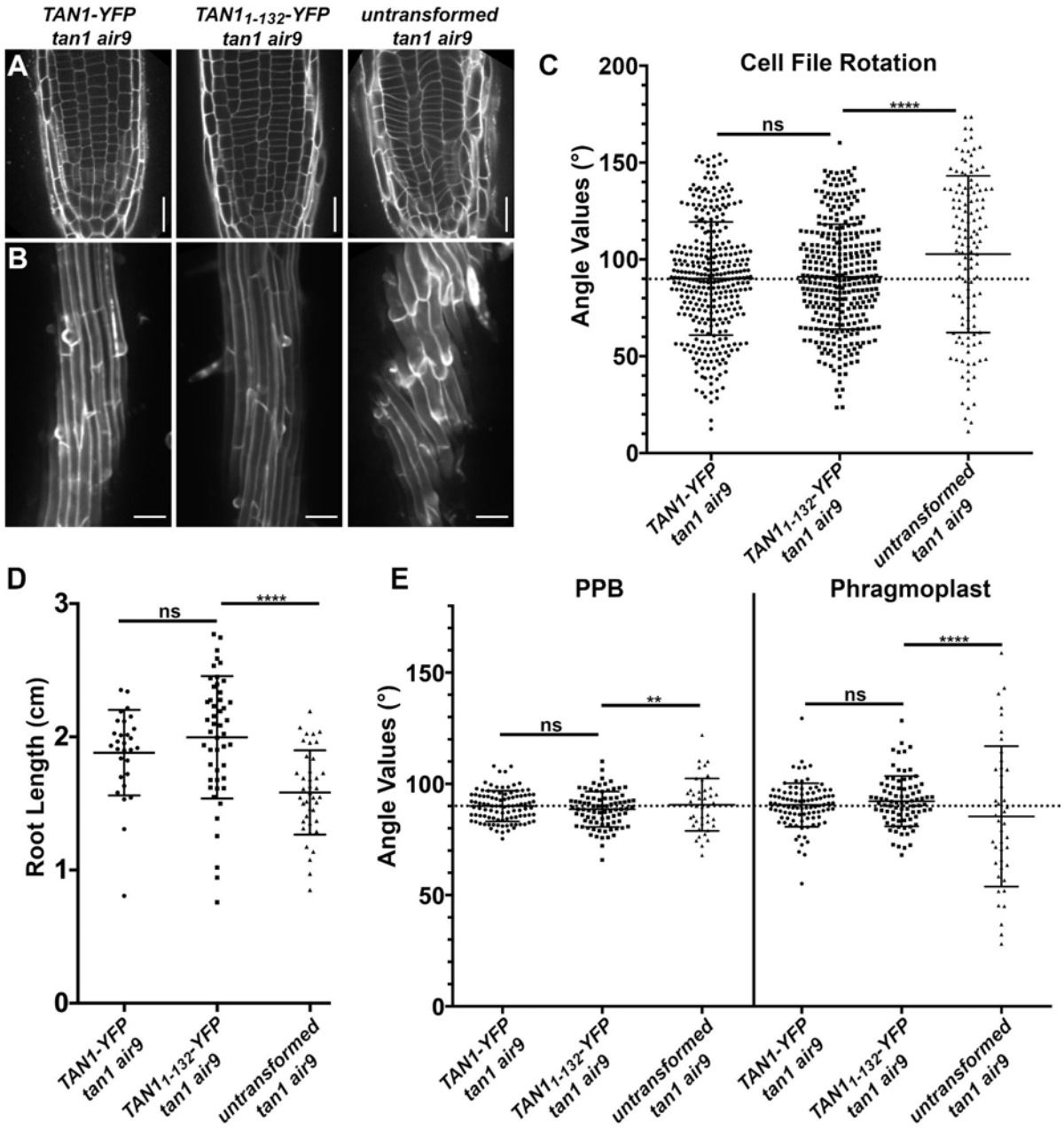

Figure 1. *p35S:TAN1$_{1-132}$-YFP* rescues Arabidopsis *tan1 air9* double mutant phenotypes. A) Cell walls stained with propidium iodide (PI) of *tan1 air9* double mutant root tips expressing *p35S:TAN1-YFP* (left), *p35S:TAN1$_{1-132}$-YFP* (middle), and untransformed *tan1 air9* double mutants (right). Bars = 25 µm. B) Maximum projections of 10 1-µm Z-stacks of PI-stained differentiation zone root cell walls. Bars = 50 µm. C) Cell file rotation angles of *tan1 air9* double mutants expressing *p35S:TAN1-YFP* (left), *p35S:TAN1$_{1-132}$-YFP* (middle) and untransformed plants (right), n > 13 plants for each genotype. Each dot represents an angle measured from the left side of the long axis of the root to the transverse cell wall. Angle variances were compared with Levene's test. D) Root length measurements from 8 days after stratification of *tan1 air9*

467 double mutants expressing *p35S:TAN1-YFP* (left), *p35S:TAN1*$_{1-132}$*-YFP* (middle) and
468 untransformed plants (right), n > 28 plants for each genotype, compared by two-tailed t-test with
469 Welch's correction. E) PPB and phragmoplast angle measurements in *tan1 air9* double mutant
470 cells expressing *p35S:TAN1-YFP* (left), *p35S:TAN1*$_{1-132}$*-YFP* (middle) and untransformed plants
471 (right), n > 20 plants for each genotype. Angle variations compared with F-test. ns indicates not
472 significant, ** P-value <0.01, **** P-value <0.0001.

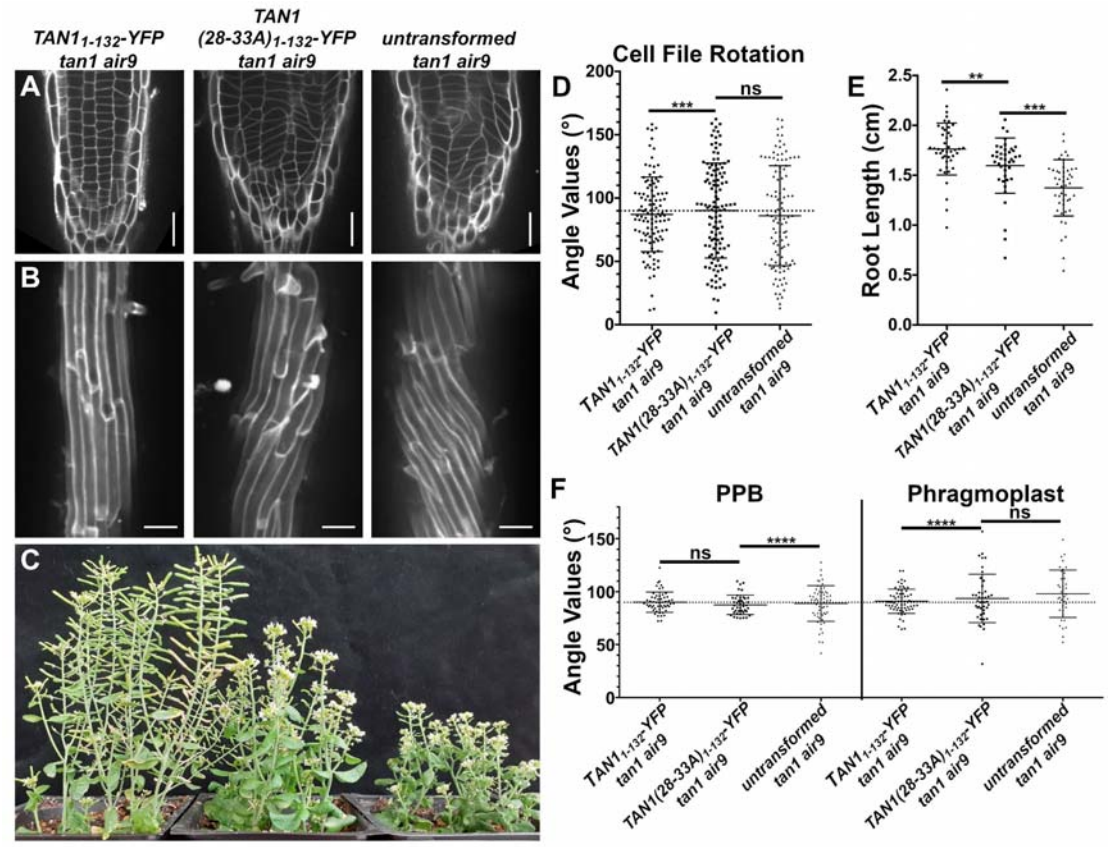

Figure 2: *p35S:TAN1(28-33A)$_{1-132}$-YFP* partially rescues *tan1 air9* double mutant phenotypes.

A) Cell walls of Arabidopsis *tan1 air9* double mutant root tips stained with propidium iodide (PI) of plants expressing *p35S:TAN1$_{1-132}$-YFP* (left), *p35S:TAN1(28-33A)$_{1-132}$-YFP* (middle), and untransformed *tan1 air9* double mutants (right). Bars = 25 µm. B) Maximum projections of 10 1-µm Z-stacks of PI-stained differentiation zone root cell walls. Bars = 50 µm. C) 58-day old *tan1 air9* double mutants expressing *p35S:TAN1$_{1-132}$-YFP* (left), *p35S:TAN1(28-33A)$_{1-132}$-YFP* (middle), and untransformed *tan1 air9* double mutants (right). D) Cell file rotation angles of *tan1 air9* double mutants expressing *p35S:TAN1$_{1-132}$-YFP* (left), *p35S:TAN1(28-33A)$_{1-132}$-YFP* (middle), and untransformed *tan1 air9* double mutants (right) n > 27 plants for each genotype. Variances were compared with Levene's test. E) Root length measurements from 8 days after stratification of *tan1 air9* double mutants expressing *p35S:TAN1$_{1-132}$-YFP* (left), *p35S:TAN1(28-33A)$_{1-132}$-YFP* (middle), and untransformed *tan1 air9* double mutants (right), n > 40 plants for each genotype, two-tailed t-test with Welch's correction. F) PPB and phragmoplast angle measurements in dividing root cells of *tan1 air9* double mutants expressing *p35S:TAN1$_{1-132}$-YFP* (left), *p35S:TAN1(28-33A)$_{1-132}$-YFP* (middle), and untransformed plants (right), n > 17 plants for each genotype. Angle variance compared with F-test. ns indicates not significant, ** P-value <0.01, *** P-value <0.001, **** P-value <0.0001.

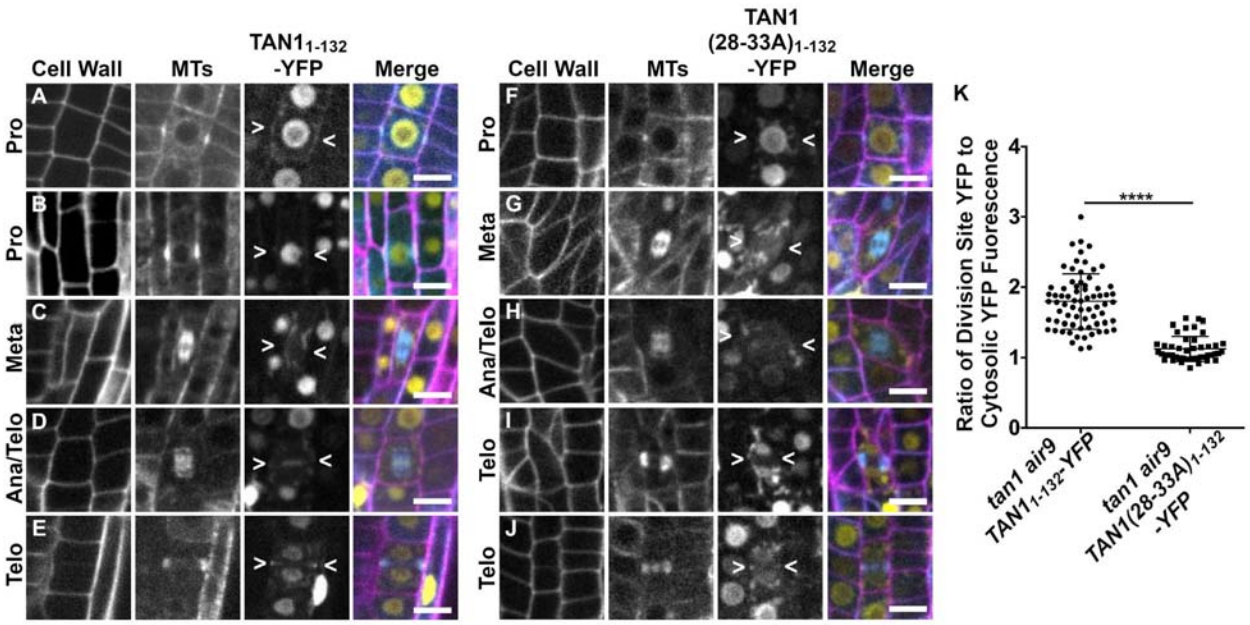

Figure 3: Division site localization during telophase is common for TAN1$_{1-132}$-YFP but rare for TAN1(28-33A)$_{1-132}$-YFP in *tan1 air9* double mutants. A-E) Propidium iodide stained *tan1 air9* plants expressing *p35S:TAN1$_{1-132}$-YFP* during mitosis (n = 29 plants). The division site is indicated by arrowheads in the YFP panels. Bars = 10 µm. A) Rare prophase division site accumulation of TAN1$_{1-132}$-YFP, (10% of cells, n = 9/89), (B) common prophase TAN1$_{1-132}$-YFP nuclear accumulation without division site localization (90%, n = 80/89), (C) no specific TAN1$_{1-132}$-YFP division site accumulation in metaphase (100% n = 28/28), (D) faint TAN1$_{1-132}$-YFP division site accumulation accompanied by midline accumulation in late anaphase/early telophase (80% of cells, n = 16/20) and E) TAN1$_{1-132}$-YFP division site accumulation during telophase (100%, n = 58/58). F-H) *tan1 air9* plants expressing *p35S:TAN1(28-33A)$_{1-132}$-YFP* during mitosis (n = 13 plants). The division site is indicated by arrowheads in the YFP panels. F) No specific TAN1(28-33A)$_{1-132}$-YFP prophase division site accumulation during prophase (100%, n = 20/20), (G) no specific TAN1(28-33A)$_{1-132}$-YFP division site accumulation during metaphase (100%, n = 12/12), (H) no TAN1(28-33A)$_{1-132}$-YFP division site or midline accumulation in late anaphase/early telophase (100% of cells, n = 8/8), (I) no specific TAN1(28-33A)$_{1-132}$-YFP division site accumulation during telophase (68% n = 15/22) and (J) faint TAN1(28-33A)$_{1-132}$-YFP division site accumulation during telophase (32%, n = 7/22). K) Ratio of TAN1$_{1-132}$-YFP (left) or TAN1(28-33A)$_{1-132}$-YFP (right) fluorescence at the division site to cytosolic fluorescence from *tan1 air9* plants expressing *p35S:TAN1$_{1-132}$-YFP* or *p35S:TAN1(28-33A)$_{1-132}$-YFP* during telophase, n >23 plants for each genotype. Asterisks indicate a significant difference as determined by Mann-Whitney U test, P-value <0.0001.

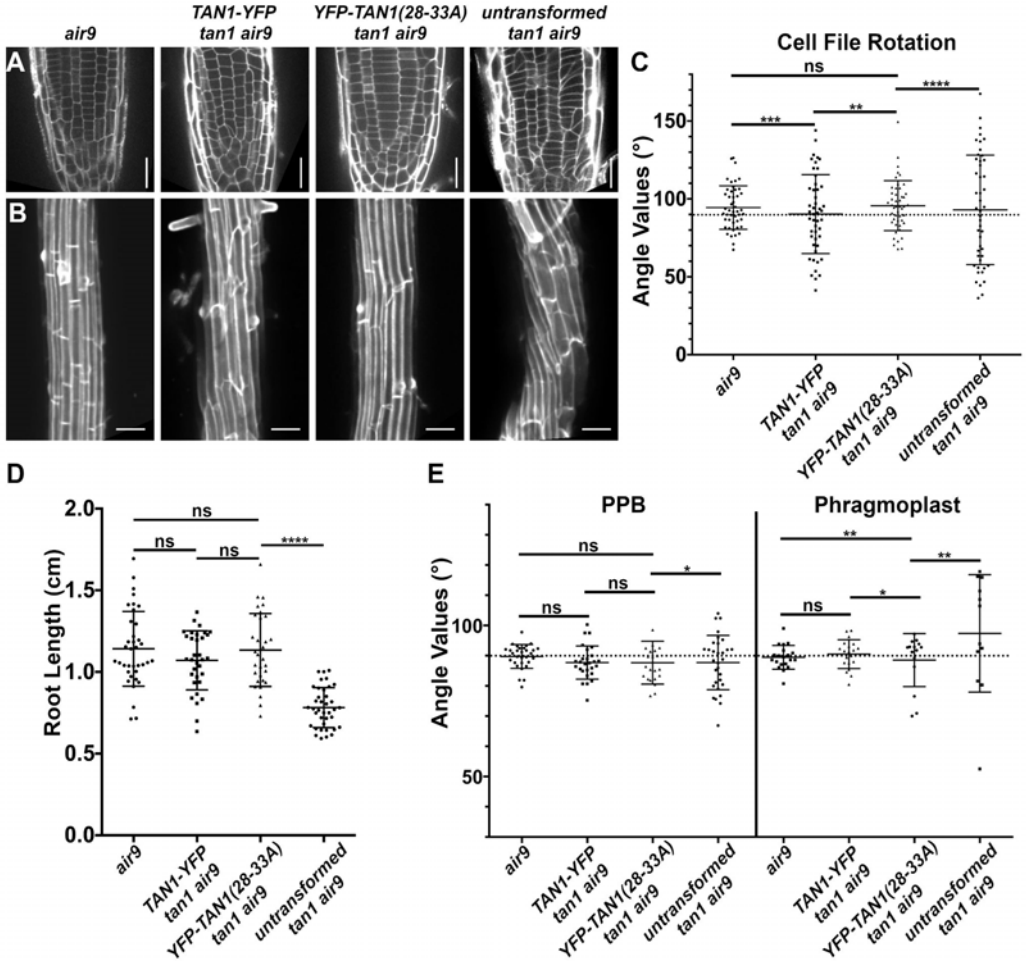

Figure 4: Full length *TAN1* with alanine substitutions replacing amino acids 28 to 33 (*p35S:YFP-TAN1(28-33A)*) mostly rescues the t*an1 air9* double mutant. A) Propidium iodide stained root tips of an *air9* single mutant (left) and *tan1 air9* double mutants expressing *p35S:TAN1-YFP* (center left) or *p35S:YFP-TAN1(28-33A)* (center right), and an untransformed *tan1 air9* plant (right). Scale bar = 25 µm. B) Maximum projections of 10 1-µm Z-stacks of PI-stained cell walls in the root differentiation zone. Bars = 50 µm. C) Cell file rotation angles of *air9* single mutants (left), *tan1 air9* double mutant plants expressing *p35S:TAN1-YFP* (center left) or *p35S:YFP-TAN1(28-33A)* (center right), and untransformed *tan1 air9* plants (right), n > 9 plants for each genotype. Variances were compared with Levene's test. D) Root length measurements from 8 days after stratification of *air9* single mutants (left) and *tan1 air9* double mutants expressing *p35S:TAN1-YFP* (center left) or *p35S:YFP-TAN1(28-33A)* (center right), and untransformed *tan1 air9* plants (right), n > 30 plants of each genotype, compared by two-tailed t-test with Welch's correction. E) PPB and phragmoplast angle measurements in dividing root cells of *air9* single mutants (left) and *tan1 air9* double mutant plants expressing *p35S:TAN1-YFP* (center left) or *p35S:YFP-TAN1(28-33A)* (center right), and untransformed *tan1 air9* plants (right), PPB measurements n > 15 plants for each genotype; phragmoplast measurements n > 8 plants for each genotype. Angle variance compared with F-test. ns

543 indicates not significant, * P-value <0.05, ** P-value <0.01, *** P-value <0.001, **** P-value
544 <0.0001.

545

546

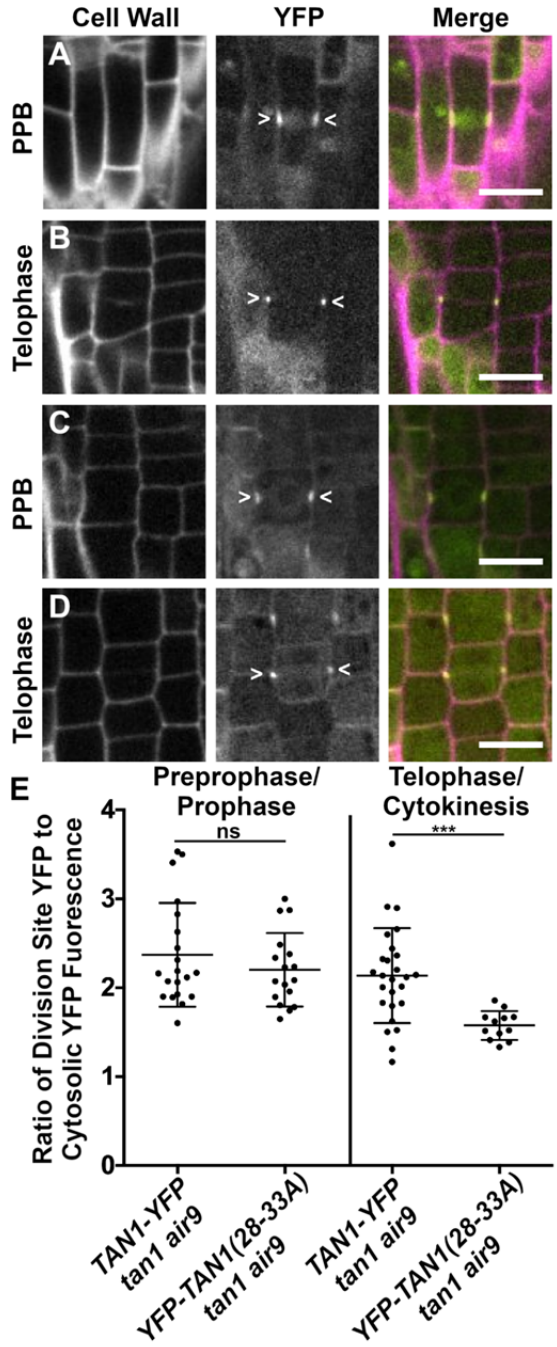

Figure 5: YFP-TAN1(28-33A) localizes normally to the division site in preprophase/prophase and with reduced fluorescence during telophase in *tan1 air9* mutants. Propidium iodide stained *tan1 air9* plants expressing *p35S:TAN1-YFP* in (A) preprophase/prophase (B) telophase/cytokinesis. *tan1 air9* plants expressing *p35S:YFP-TAN1(28-33A)* in (C) preprophase or prophase (D) telophase/cytokinesis. The division site is indicated by arrowheads in the YFP panels. Bars = 10 μm. E) TAN1-YFP or TAN1(28-33A)-YFP ratio of the division site versus cytosolic fluorescence intensity from *tan1 air9* plants expressing *p35S:TAN1-YFP* or *p35S:YFP-TAN1(28-33A)* during preprophase/prophase and telophase/cytokinesis, n >5 plants for each genotype. Ratios compared with Mann-Whitney U test, P-value <0.001.

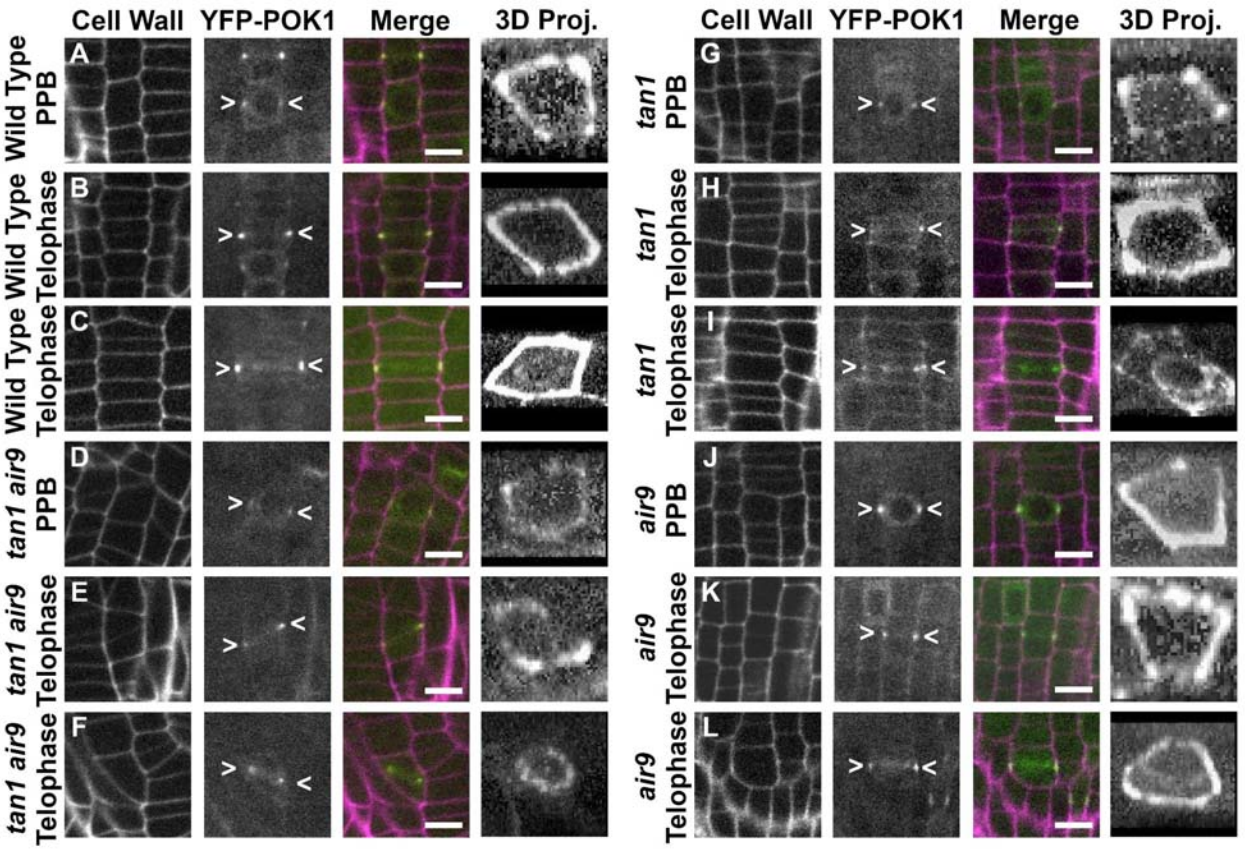

FIGURE 6: TAN1 and AIR9 together promote POK1 localization to the division site during telophase. YFP-POK1 localization in propidium iodide stained Col-0 wild type plants, *tan1* single mutants, *air9* single mutants, and *tan1 air9* double mutants. Bars = 10 µm. "3D Proj." panels show 3D projections rotated to show the YFP-POK1 rings at the cortex or the phragmoplast in the corresponding cells in each row. A-C) YFP-POK1 localization in Col-0 wild type plants (n = 17 plants). A) YFP-POK1 localization during preprophase/prophase (n = 40 cells). B) YFP-POK1 was observed at the division site in telophase cells (n = 76 cells). C) In 4% of telophase cells (n = 3/76), YFP-POK1 accumulated both in the phragmoplast midline and at the division site. D-F) YFP-POK1 localization in *tan1 air9* double mutant plants, n = 9 plants. D) YFP-POK1 localization during preprophase/prophase (n=17 cells). E) YFP-POK1 was also observed at the cortex in telophase cells (n=9/23 cells). F) In 61% of telophase cells, YFP-POK1 accumulated at the midline but was absent from the cortex (n=14/23 cells). G-I) YFP-POK1 localization in *tan1* single mutants, n = 6 plants. G) YFP-POK1 localization during preprophase/prophase (n = 10 cells). (H) YFP-POK1 was observed at the division site in telophase cells (n = 27 cells). I) In 26% of telophase cells (n = 7/27), YFP-POK1 accumulated both in the phragmoplast midline and at the division site. J-L) YFP-POK1 localization in *air9* single mutants, n = 6 plants. J) YFP-POK1 localization during preprophase/prophase (n = 12 cells). K) YFP-POK1 was observed at the division site in telophase cells (n=18 cells). L) In 17% of telophase cells (n = 3/18), YFP-POK1 accumulated both in the phragmoplast midline and at the division site.

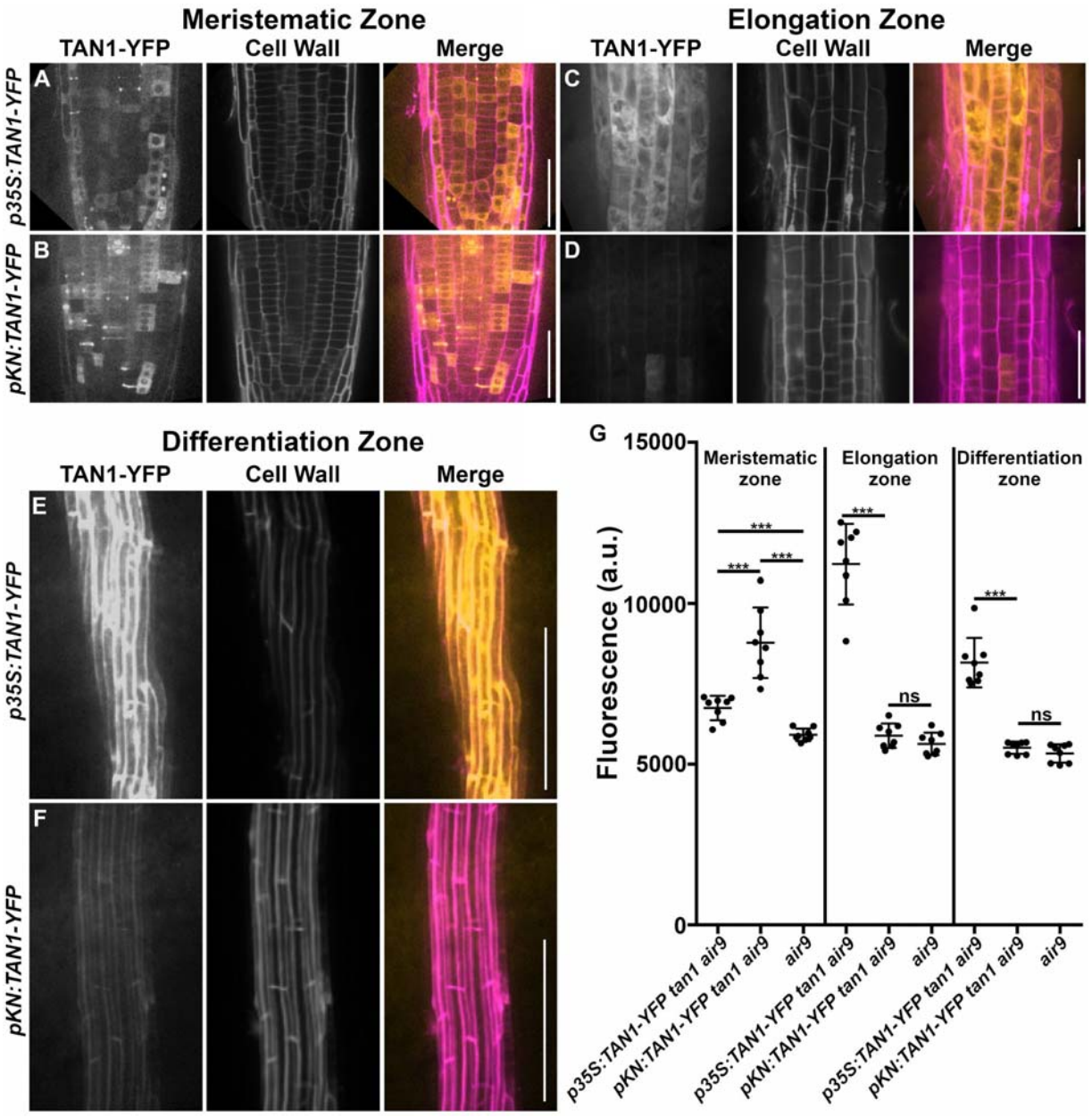

Figure 7: Comparison of TAN1-YFP expression driven by the cauliflower mosaic virus *35S* promoter and G2/M specific *KNOLLE* promoter in the roots of *tan1 air9* double mutants. (A and B) Micrographs of the meristematic zone, (C and D) elongation zone, and (E and F) differentiation zone of *tan1 air9* double mutants expressing (A, C, E) *p35S:TAN1-YFP* or (B, D, F) *pKN:TAN1-YFP*. Cell walls were stained with propidium iodide. Root tip and elongation zone, bars = 50µm and differentiation zone, bars = 200µm. G) Fluorescence intensity measurements (arbitrary units, a.u. of TAN1-YFP) from the meristematic zone, elongation zone, and differentiation zone of *tan1 air9* double mutants expressing *p35S:TAN1-YFP* (left), *pKN:TAN1-YFP* (middle), and *air9* single mutants, n > 7 plants for each genotype, fluorescence compared with Mann-Whitney U test, P-value <0.001. ns indicates not significant.

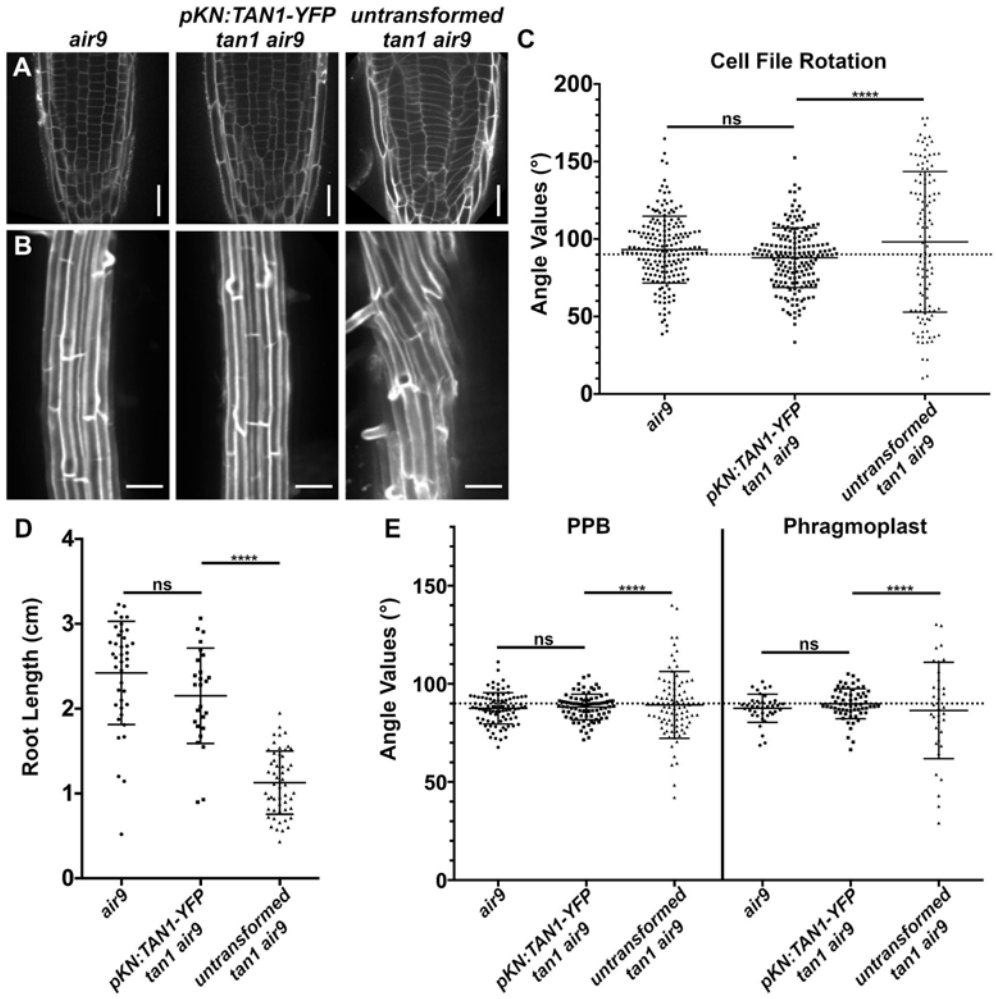

Figure 8. Full rescue of the *tan1 air9* double mutant with the mitosis specific promoter from *KNOLLE* fused to full length TAN1 (*pKN:TAN1-YFP*). A) Propidium iodide (PI) stained root tips of an *air9* single mutant (left), *tan1 air9* double mutant expressing *pKN:TAN1-YFP* (middle), and untransformed *tan1 air9* plant (right). Bars = 25 µm. B) Maximum projections of 10 1-µm Z-stacks of PI-stained differentiation zone root cell walls. Bars = 50 µm. C) Cell file rotation angles of *air9* single mutants (left), *tan1 air9* double mutants expressing *pKN:TAN1-YFP* (middle), and untransformed plants (right), n > 23 plants for each genotype. Angle variances were compared with Levene's test. D) Root length measurements from 8 days after stratification of *air9* single mutants (left), *tan1 air9* double mutants expressing *pKN:TAN1-YFP* (middle), and untransformed plants (right), n > 25 plants for each genotype, compared by two-tailed t-test with Welch's corrections. E) PPB and phragmoplast angle measurements in *air9* single mutants (left), *tan1 air9* double mutants expressing *pKN:TAN1-YFP* (middle), and untransformed *tan1 air9* plants (right), n > 20 plants for each genotype. Angle variations compared with F-test. ns indicates not significant, **** P-value <0.0001.

Supplementary Figures

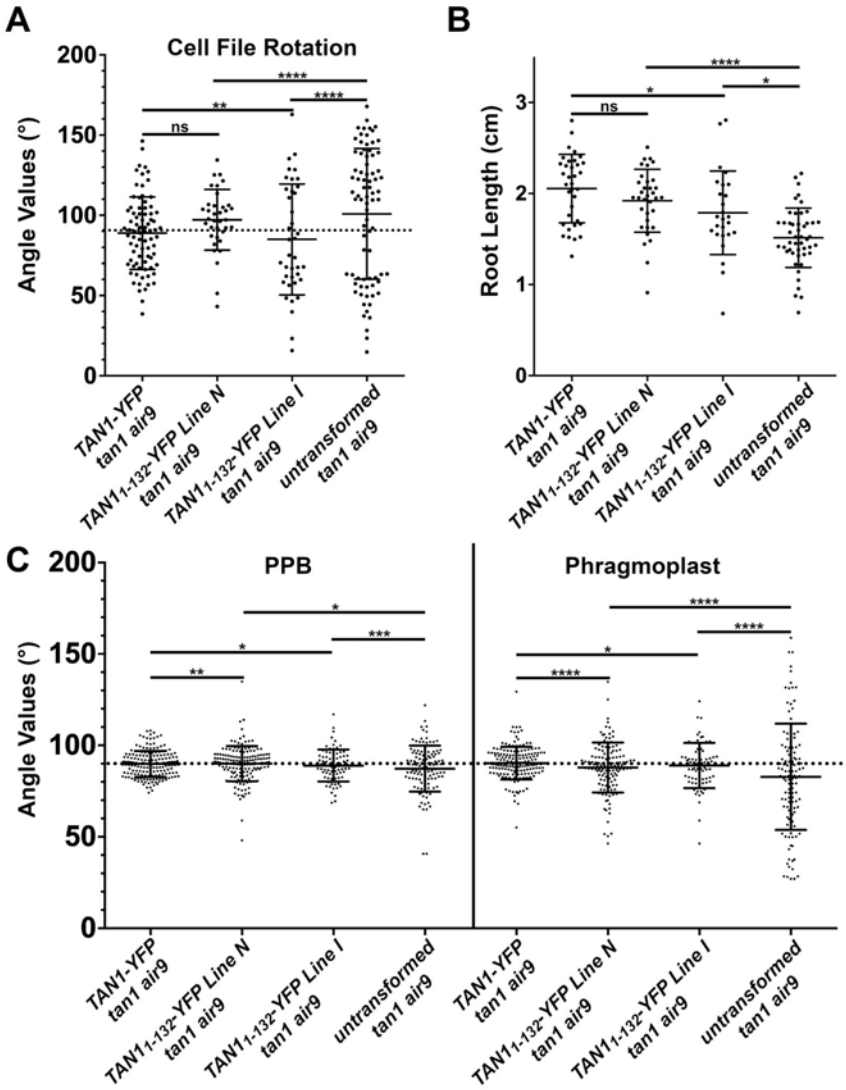

Supplementary Figure 1. *p35S:TAN1$_{1-132}$-YFP tan1 air9* lines show significant rescue compared to untransformed *tan1 air9* double mutants. A) Cell file rotation angles of *tan1 air9* double mutants expressing *p35S:TAN1-YFP* (left), two *p35S:TAN1$_{1-132}$-YFP* transgenic lines designated as line N (center left) and line I (center right) and untransformed *tan1 air9* plants (right) n > 6 plants for each genotype. Angle variances were compared with Levene's test. B) Root length measurements from 8 days after stratification of *tan1 air9* double mutants expressing *p35S:TAN1-YFP* (left), two *p35S:TAN1$_{1-132}$-YFP* transgenic lines (middle) and untransformed plants (right), n > 13 plants for each genotype, compared by two-tailed t-test with Welch's correction. C) PPB and phragmoplast angle measurements in dividing root cells of *tan1 air9* double mutants expressing *p35S:TAN1-YFP* (left), two *p35S:TAN1$_{1-132}$-YFP* transgenic lines (middle) and untransformed plants (right), n > 23 plants of each genotype. Angle variations compared with F-test. ns indicates not significant, * P-value <0.05,** P-value <0.01, **** P-value <0.0001.

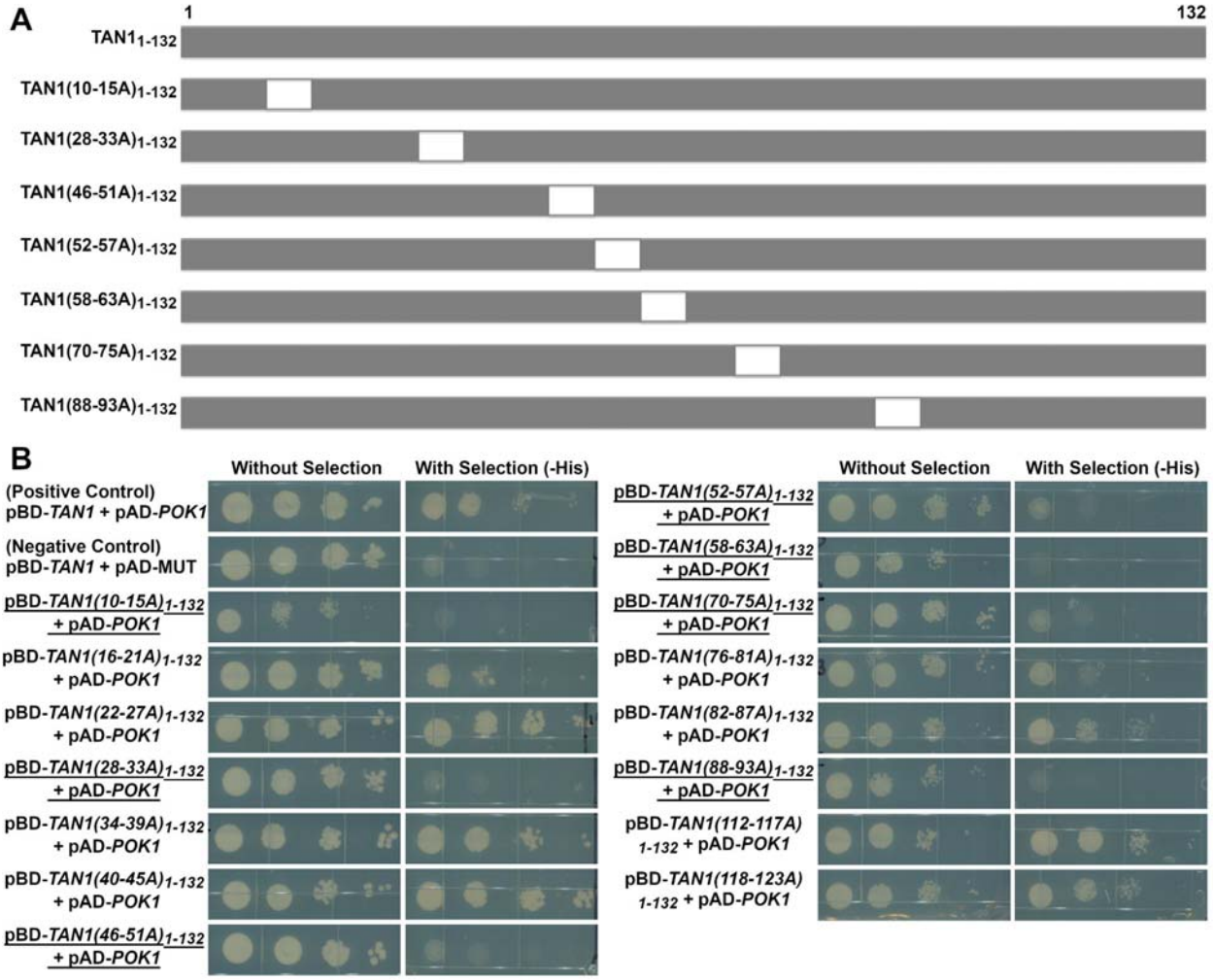

Supplementary Figure 2. Yeast two-hybrid interactions between POK1 (C-terminal amino acids 1683-2066, as previously described (Müller et al., 2006; Rasmussen et al., 2011; Lipka et al., 2014) **) and $TAN1_{1-132}$ alanine scanning constructs.** A) Diagram of alanine scanning constructs that showed loss of interaction with POK1 by yeast two-hybrid. The location of the six alanine substitutions within each $TAN1_{1-132}$ construct are represented by white boxes. B) Yeast two-hybrid results of screen for loss of interaction with POK1. Underlined constructs showed loss of interaction with POK1.

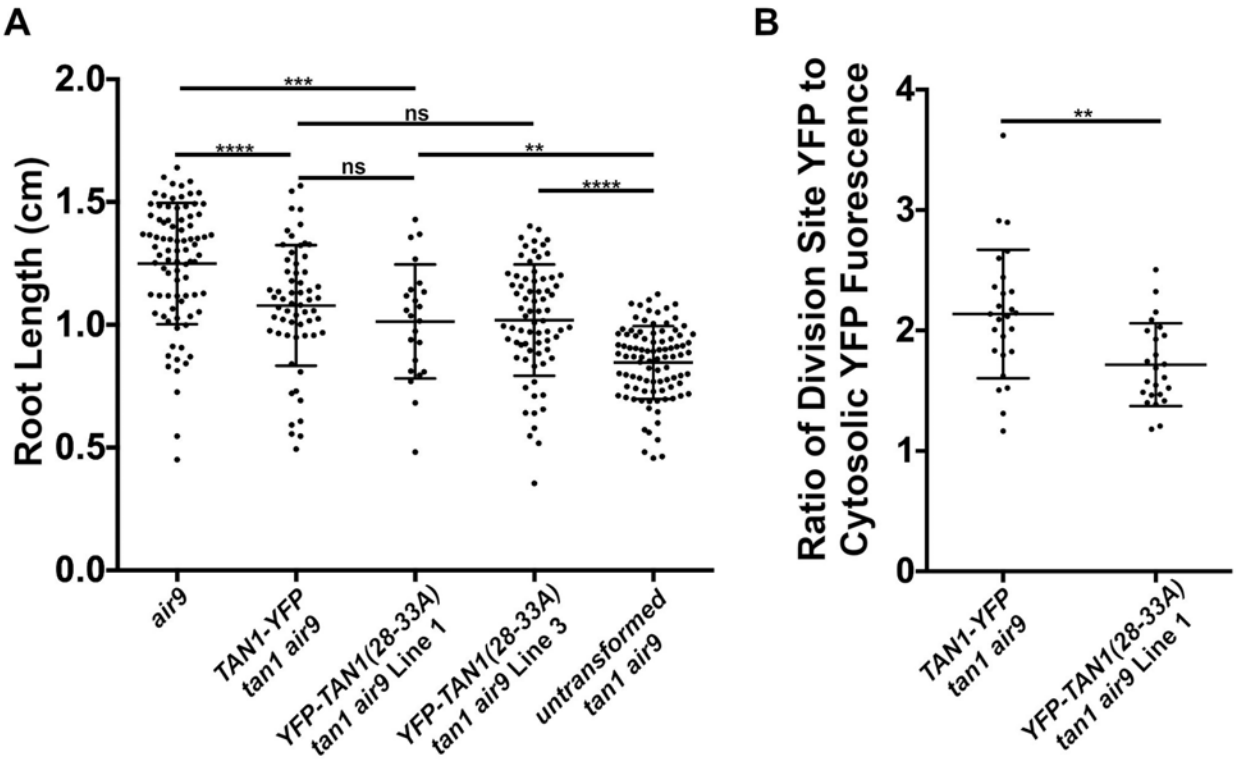

Supplementary Figure 3. ***p35S:YFP-TAN1(28-33A) tan1 air9*** **lines show significant rescue compared to untransformed** ***tan1 air9,*** **but less accumulation of YFP-TAN1(28-33A) during telophase.** A) Root length measurements from 8 days after stratification of *air9* single mutants (left), *tan1 air9* double mutants expressing *p35S:TAN1-YFP* (second from the left), two *p35S:YFP-TAN1(28-33A)-YFP* transgenic lines designated as line 1 (center) and line 3 (second from the right), and untransformed plants (right), n > 22 plants for each genotype, compared by two-tailed t-test with Welch's correction. B) Ratio of TAN1-YFP or TAN1(28-33A)-YFP fluorescence at the division site to cytosolic fluorescence from *tan1 air9* plants expressing *p35S:TAN1-YFP* (left) or *p35S:YFP-TAN1(28-33A)* (right) during telophase, n >12 plants for each genotype. Asterisks indicate a significant difference as determined by Mann-Whitney U test, P-value <0.01. Note: TAN1-YFP fluorescence measurements are the same as those used for the telophase fluorescence measurements in Figure 5E.

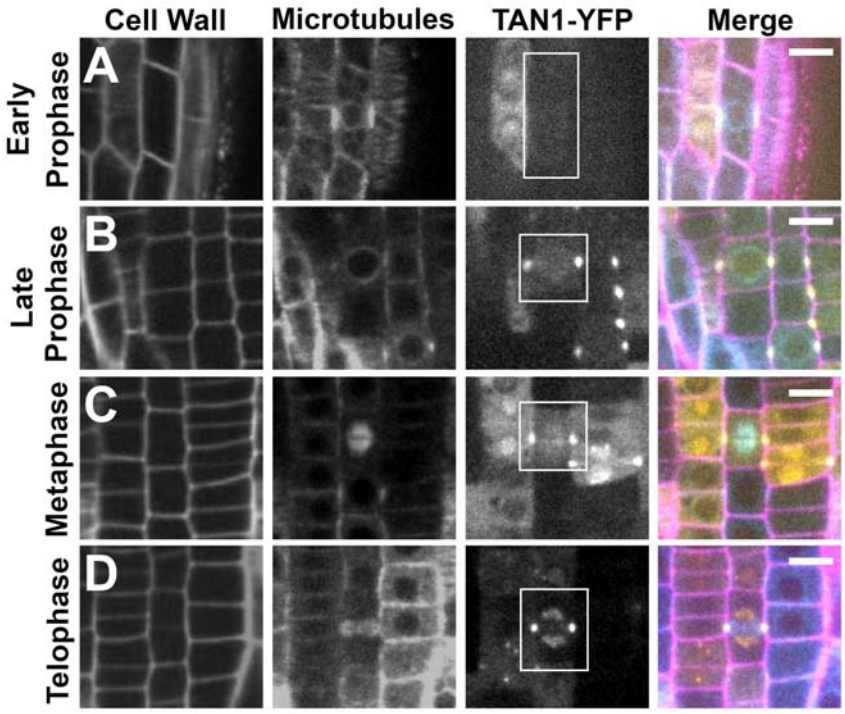

Supplementary Figure 4. Division site localization of TAN1-YFP driven by the *KNOLLE* promoter in *tan1 air9* double mutants. Confocal images of propidium iodide-stained roots of *tan1 air9* plants expressing *CFP-TUBULIN* and *pKN:TAN1-YFP* in dividing root tip cells. Representative images of cells with a (A) broad early PPB, (B) late narrow PPB, (C) metaphase spindle, and (D) phragmoplast. Bars = 10 μm. White boxes in the TAN1-YFP channel outline the relevant cell for the row.

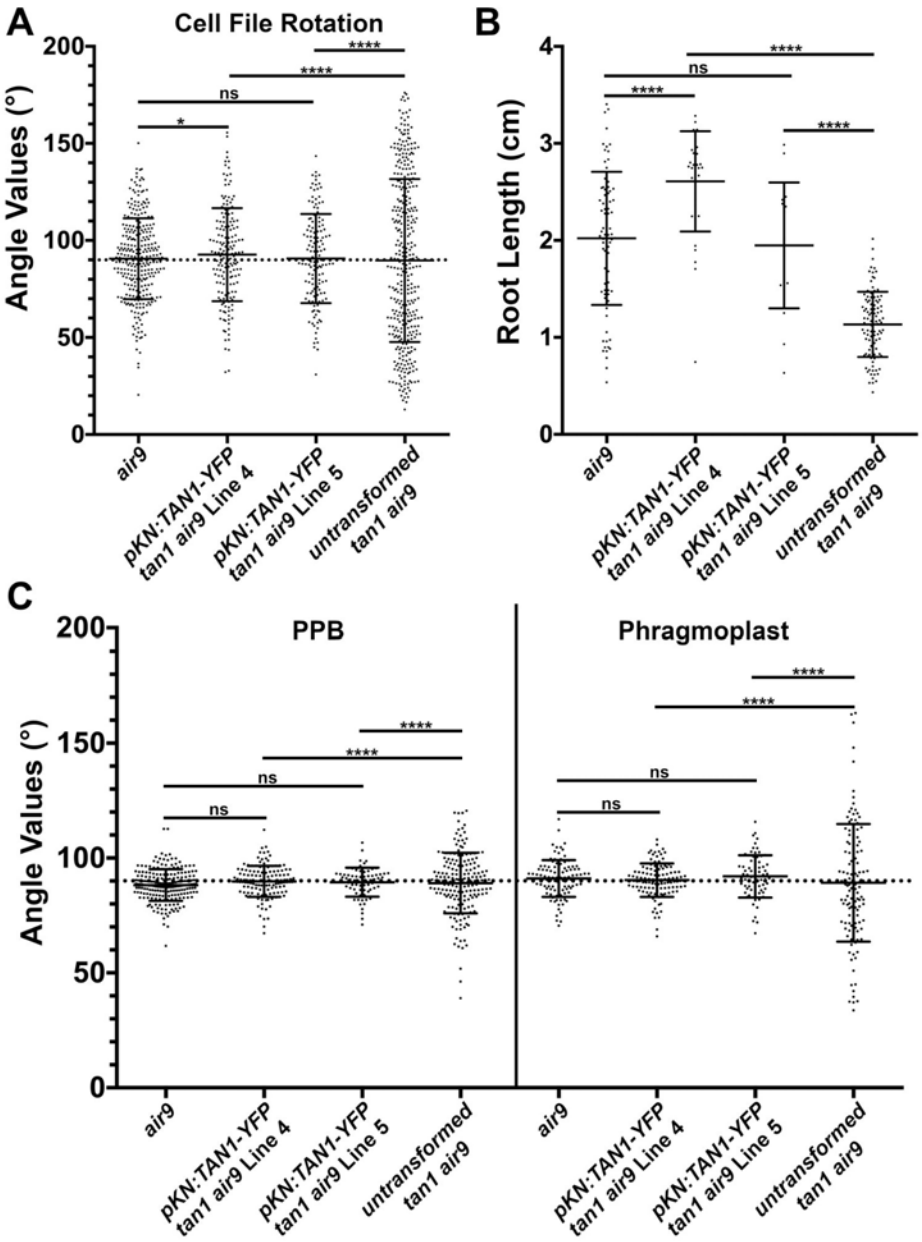

Supplementary Figure 5. *pKN:TAN1$_{1-132}$-YFP tan1 air9* lines show significant rescue compared to untransformed *tan1 air9.* A) Cell file rotation angles of *air9* single mutants (left), two transgenic lines expressing *pKN:TAN1-YFP* in the *tan1 air9* double mutant designated as line 4 (center left) and line 5 (center right) and untransformed plants (right), n >17 plants for each genotype. Angle variance were compared with Levene's test. B) Root length measurements from 8 days after stratification of *air9* single mutants (left), two transgenic lines expressing *pKN:TAN1-YFP* in the *tan1 air9* double mutant (middle), and untransformed plants (right), n > 21 plants for each genotype, compared by two-tailed t-test with Welch's correction. C) PPB and phragmoplast angle measurements in dividing root cells of *air9* single mutants (left), two transgenic lines expressing *pKN:TAN1-YFP* in the *tan1 air9* double mutant (middle), and untransformed plants (right), n > 15 plants for each genotype. Angle variations compared with F-test. ns indicates not significant, **** P-value <0.0001.

691

692 **Supplementary Table 1. Primers used for cloning and genotyping.**

693

Primer Name	Sequence
ATRP	ATCTCTTAGGAACCAAAACCGGACGCTGT
ATLP	GATCCGTTACGAAAGTGAACACCTTTATC
JL202	CATTTTATAATAACGCTGCGGACATCTAC
AIR9-5RP	TGGATCAGCTGCAACATTATTC
AIR9-5LP	ATTAACATTTTGCAACGCAGG
LBb1.3	ATTTTGCCGATTTCGGAAC
Ds5-4	TACGATAACGGTCGGTACGG
AtTAN 733-CDS Rw	AAATAGAGGGTTCGGAAAAAGAACC
AIR9 gnm7511 R	CCTCCAGTATATGAAGCAACAAAGC
AIR9_cDNA 2230 F	GATGAGGAATATATGTTATCTTTAGATG
pKN-5'SacI Fw	gaggagctccagaagaaaaagaaaaagttctc
pKN-5'EcoRI Rw	TAAGCGGAATTCCTTTTTCACCTGAAA
35SpKN5' Fw	ACCCACAGATGGTTAGAGagg
YFP XhoI Rw	ATAATGCTCGAGAGAGTCGCG
Ala_Scan_FOR	GCCGTCACAGATAGATTGGCT
Ala_Scan_Rev	GAAAGCAACCTGACCTACAGG
Ala_02_FOR	GCTGCTGCCGCTGCCGCTGTGCCTCCTCTCAACTCAGAT
Ala_02_Rev	AGCGGCAGCGGCAGCAGCCTGCTTCTGTGGGGTTCT
Ala_03_FOR	GCTGCTGCCGCTGCCGCTGATCTTCTCAAGGAAACGATCAAC
Ala_03_REV	AGCGGCAGCGGCAGCAGCCACCATCGCCACTTTCCT
Ala_04_FOR	GCTGCTGCCGCTGCCGCTATCAACAAGGTTGATAAATGTATGGAA
Ala_04_REV	AGCGGCAGCGGCAGCAGCTGAGTTGAGAGGAGGCACCAC
Ala_05_FOR	GCTGCTGCCGCTGCCGCTTGTATGGAAAGACTGCAAGAGCTA
Ala_05_REV	AGCGGCAGCGGCAGCAGCCGTTTCCTTGAGAAGATCTGAGTT
Ala_06_FOR	GCTGCTGCCGCTGCCGCTGAGCTACAGTACACAATTGCAGGA
Ala_06_REV	AGCGGCAGCGGCAGCAGCTTTATCAACCTTGTTGATCGTTTCCTT
Ala_07_FOR	GCTGCTGCCGCTGCCGCTGCAGGAGGAACCAAAGTTGTC
Ala_07_REV	AGCGGCAGCGGCAGCAGCTTGCAGTCTTTCCATACATTTATCAAC
Ala_08_FOR	GCTGCTGCCGCTGCCGCTGTCTCTGGTGTGAACCTTAGC
Ala_08_REV	AGCGGCAGCGGCAGCAGCAATTGTGTACTGTAGCTCTTGCAG
Ala_09_FOR	GCTGCTGCCGCTGCCGCTAGCCCTCGAAGCACTAGA
Ala_09_REV	AGCGGCAGCGGCAGCAGCAACTTTGGTTCCTCCTGCAAT
Ala_10_FOR	GCTGCTGCCGCTGCCGCTATTTACTTGAAGACTAGTCTTAGATGCAAG
Ala_10_REV	AGCGGCAGCGGCAGCAGCAAGGTTCACACCAGAGACAAC
Ala_12_FOR	GCTGCTGCCGCTGCCGCTACTTTAAGGATCAAGAATGCTACTAATAAG
Ala_12_REV	AGCGGCAGCGGCAGCAGCACTAGTCTTCAAGTAAATTCTAGTGCT
Ala_13_FOR	GCTGCTGCCGCTGCCGCTGCTACTAATAAGAAATCTCCAGTAGGG
Ala_13_REV	AGCGGCAGCGGCAGCAGCTTCTTGCTTGCATCTAAGACTAGT
Ala_14_FOR	GCTGCTGCCGCTGCCGCTCCAGTAGGGAAGTTTCCTGCT
Ala_14_REV	AGCGGCAGCGGCAGCAGCATTCTTGATCCTTAAAGTTTCTTGCTT
Ala_15_FOR	GCTGCTGCCGCTGCCGCTGCTTCCTCACCAGGAGATTGG
Ala_15_REV	AGCGGCAGCGGCAGCAGCAGATTTCTTATTAGTAGCATTCTTGATCCT
Ala_16_FOR	GCTGCTGCCGCTGCCGCTTGGAGGAAAATGTCACTCCCA
Ala_16_REV	AGCGGCAGCGGCAGCAGCAGGAAACTTCCCTACTGGAGA
Ala_17_FOR	GCTGCTGCCGCTGCCGCTCCAGCAATGCTACTAGGAGAG
Ala_17_REV	AGCGGCAGCGGCAGCAGCATCTCCTGGTGAGGAAGCAGG
Ala_19_FOR	GCTGCTGCCGCTGCCGCTTTACAAGCCTCACAGGTCACA
Ala_19_REV	AGCGGCAGCGGCAGCAGCTCCTAGTAGCATTGCTGGGAG
Ala_20_FOR	GCTGCTGCCGCTGCCGCTACAAGAGACATTGTGGACGCC
Ala_20_REV	AGCGGCAGCGGCAGCAGCGATTTCATTTACAGTCTCTCCTAGTAGCAT

694

695

696

697

Parsed Citations

Abe, T., Thitamadee, S., and Hashimoto, T. (2004). Microtubule defects and cell morphogenesis in the lefty1lefty2 tubulin mutant of Arabidopsis thaliana. Plant Cell Physiol. 45: 211–220.
Google Scholar: Author Only Title Only Author and Title

Bellinger, M.A., Uyehara, A.N., Martinez, P., McCarthy, M.C., and Rasmussen, C.G. (2021). Cell cortex microtubules contribute to division plane positioning during telophase in maize. Cold Spring Harbor Laboratory: 2021.01.11.426230.
Google Scholar: Author Only Title Only Author and Title

Buschmann, H. and Borchers, A. (2020). Handedness in plant cell expansion: a mutant perspective on helical growth. New Phytol. 225: 53–69.
Google Scholar: Author Only Title Only Author and Title

Buschmann, H., Chan, J., Sanchez-Pulido, L., Andrade-Navarro, M.A., Doonan, J.H., and Lloyd, C.W. (2006). Microtubule-associated AIR9 recognizes the cortical division site at preprophase and cell-plate insertion. Curr. Biol. 16: 1938–1943.
Google Scholar: Author Only Title Only Author and Title

Buschmann, H., Dols, J., Kopischke, S., Peña, E.J., Andrade-Navarro, M.A., Heinlein, M., Szymanski, D.B., Zachgo, S., Doonan, J.H., and Lloyd, C.W. (2015). Arabidopsis KCBP interacts with AIR9 but stays in the cortical division zone throughout mitosis via its MyTH4-FERM domain. J. Cell Sci. 128: 2033–2046.
Google Scholar: Author Only Title Only Author and Title

Buschmann, H., Fabri, C.O., Hauptmann, M., Hutzler, P., Laux, T., Lloyd, C.W., and Schäffner, A.R. (2004). Helical Growth of the Arabidopsis Mutant tortifolia1 Reveals a Plant-Specific Microtubule-Associated Protein. Curr. Biol. 14: 1515–1521.
Google Scholar: Author Only Title Only Author and Title

Buschmann, H., Hauptmann, M., Niessing, D., Lloyd, C.W., and Scha, A.R. (2009). Helical Growth of the Arabidopsis Mutant tortifolia2 Does Not Depend on Cell Division Patterns but Involves Handed Twisting of Isolated Cells. 21: 2090–2106.
Google Scholar: Author Only Title Only Author and Title

Chugh, M., Reißner, M., Bugiel, M., Lipka, E., Herrmann, A., Roy, B., Müller, S., and Schäffer, E. (2018). Phragmoplast Orienting Kinesin 2 Is a Weak Motor Switching between Processive and Diffusive Modes. Biophys. J. 115: 375–385.
Google Scholar: Author Only Title Only Author and Title

Cleary, A.L. and Smith, L.G. (1998). The Tangled1 Gene Is Required for Spatial Control of Cytoskeletal Arrays Associated with Cell Division during Maize Leaf Development. 10: 1875–1888.
Google Scholar: Author Only Title Only Author and Title

Clough, S.J. and Bent, A.F. (1999). Floral dip : a simplified method for Agrobacterium-mediated transformation of Arabidopsis thaliana. 16: 735–743.
Google Scholar: Author Only Title Only Author and Title

Cnops, G., Wang, X., Linstead, P., Van Montagu, M., Van Lijsebettens, M., and Dolan, L. (2000). Tornado1 and tornado2 are required for the specification of radial and circumferential pattern in the Arabidopsis root. Development 127: 3385–3394.
Google Scholar: Author Only Title Only Author and Title

Dixit, R. and Cyr, R.J. (2002). Spatio-temporal relationship between nuclear-envelope breakdown and preprophase band disappearance in cultured tobacco cells. Protoplasma 219: 116–121.
Google Scholar: Author Only Title Only Author and Title

Earley, K.W., Haag, J.R., Pontes, O., Opper, K., Juehne, T., Song, K., and Pikaard, C.S. (2006). Gateway-compatible vectors for plant functional genomics and proteomics. Plant J. 45: 616–629.
Google Scholar: Author Only Title Only Author and Title

Facette, M.R., Rasmussen, C.G., and Van Norman, J.M. (2018). A plane choice: coordinating timing and orientation of cell division during plant development. Curr. Opin. Plant Biol. 47: 47–55.
Google Scholar: Author Only Title Only Author and Title

Fan, H.Y., Hu, Y., Tudor, M., and Ma, H. (1997). Specific interactions between the K domains of AG and AGLs, members of the MADS domain family of DNA binding proteins. Plant J. 12: 999–1010.
Google Scholar: Author Only Title Only Author and Title

Goff, J. and Van Norman, J.M. (2021). Polarly localized receptor-like kinases PXC2 and IRK act redundantly during Arabidopsis root development in the radial axis. bioRxiv: 2021.02.11.429611.
Google Scholar: Author Only Title Only Author and Title

Goldy, C., Pedroza-Garcia, J.-A., Breakfield, N., Cools, T., Vena, R., Benfey, P.N., De Veylder, L., Palatnik, J., and Rodriguez, R.E. (2021). The Arabidopsis GRAS-type SCL28 transcription factor controls the mitotic cell cycle and division plane orientation. Proc. Natl. Acad. Sci. U. S. A. 118.
Google Scholar: Author Only Title Only Author and Title

Haga, N., Kobayashi, K., Suzuki, T., Maeo, K., Kubo, M., Ohtani, M., Mitsuda, N., Demura, T., Nakamura, K., Jürgens, G., and Ito, M.

(2011). Mutations in MYB3R1 and MYB3R4 cause pleiotropic developmental defects and preferential down-regulation of multiple G2/M-specific genes in Arabidopsis. Plant Physiol. 157: 706–717.
Google Scholar: Author Only Title Only Author and Title

Hashimoto, T. (2015). Microtubules in plants. Arabidopsis Book 13: e0179.
Google Scholar: Author Only Title Only Author and Title

Herrmann, A., Livanos, P., Lipka, E., Gadeyne, A., Hauser, M.-T., Van Damme, D., and Müller, S. (2018). Dual localized kinesin-12 POK2 plays multiple roles during cell division and interacts with MAP65-3. EMBO Rep. 19: e46085.
Google Scholar: Author Only Title Only Author and Title

Hoshino, H., Yoneda, A., Kumagai, F., and Hasezawa, S. (2003). Roles of actin-depleted zone and preprophase band in determining the division site of higher-plant cells, a tobacco BY-2 cell line expressing GFP-tubulin. Protoplasma 222: 157–165.
Google Scholar: Author Only Title Only Author and Title

Ishida, T., Kaneko, Y., Iwano, M., and Hashimoto, T. (2007). Helical microtubule arrays in a collection of twisting tubulin mutants of Arabidopsis thaliana. Proc. Natl. Acad. Sci. U. S. A. 104: 8544–8549.
Google Scholar: Author Only Title Only Author and Title

Karahara, I., Suda, J., Tahara, H., Yokota, E., Shimmen, T., Misaki, K., Yonemura, S., Staehelin, L.A., and Mineyuki, Y. (2009). The preprophase band is a localized center of clathrin-mediated endocytosis in late prophase cells of the onion cotyledon epidermis. Plant J. 57: 819–831.
Google Scholar: Author Only Title Only Author and Title

Kirik, V., Herrmann, U., Parupalli, C., Sedbrook, J.C., Ehrhardt, D.W., and Hülskamp, M. (2007). CLASP localizes in two discrete patterns on cortical microtubules and is required for cell morphogenesis and cell division in Arabidopsis.: 4416–4425.
Google Scholar: Author Only Title Only Author and Title

Kojo, K.H., Higaki, T., Kutsuna, N., Yoshida, Y., Yasuhara, H., and Hasezawa, S. (2013). Roles of cortical actin microfilament patterning in division plane orientation in plants. Plant Cell Physiol. 54: 1491–1503.
Google Scholar: Author Only Title Only Author and Title

Lee, Y.-R.J., Hiwatashi, Y., Hotta, T., Xie, T., Doonan, J.H., and Liu, B. (2017). The Mitotic Function of Augmin Is Dependent on Its Microtubule-Associated Protein Subunit EDE1 in Arabidopsis thaliana. Curr. Biol. 27: 3891–3897.e4.
Google Scholar: Author Only Title Only Author and Title

Lee, Y.-R.J. and Liu, B. (2019). Microtubule nucleation for the assembly of acentrosomal microtubule arrays in plant cells. New Phytol. 222: 1705–1718.
Google Scholar: Author Only Title Only Author and Title

Lee, Y.-R.J., Li, Y., and Liu, B. (2007). Two Arabidopsis phragmoplast-associated kinesins play a critical role in cytokinesis during male gametogenesis. Plant Cell 19: 2595–2605.
Google Scholar: Author Only Title Only Author and Title

Lieber, D., Lora, J., Schrempp, S., Lenhard, M., and Laux, T. (2011). Arabidopsis WIH1 and WIH2 genes act in the transition from somatic to reproductive cell fate. Curr. Biol. 21: 1009–1017.
Google Scholar: Author Only Title Only Author and Title

Lipka, E., Gadeyne, A., Stöckle, D., Zimmermann, S., De Jaeger, G., Ehrhardt, D.W., Kirik, V., Van Damme, D., and Müller, S. (2014). The Phragmoplast-Orienting Kinesin-12 Class Proteins Translate the Positional Information of the Preprophase Band to Establish the Cortical Division Zone in Arabidopsis thaliana. Plant Cell 26: 2617–2632.
Google Scholar: Author Only Title Only Author and Title

Li, S., Sun, T., and Ren, H. (2015). The functions of the cytoskeleton and associated proteins during mitosis and cytokinesis in plant cells. Front. Plant Sci. 6: 282.
Google Scholar: Author Only Title Only Author and Title

Livanos, P. and Müller, S. (2019). Division Plane Establishment and Cytokinesis. Annu. Rev. Plant Biol.
Google Scholar: Author Only Title Only Author and Title

Martinez, P., Dixit, R., Balkunde, R.S., Zhang, A., O'Leary, S.E., Brakke, K.A., and Rasmussen, C.G. (2020). TANGLED1 mediates microtubule interactions that may promote division plane positioning in maize. J. Cell Biol. 219.
Google Scholar: Author Only Title Only Author and Title

Martinez, P., Luo, A., Sylvester, A., and Rasmussen, C.G. (2017). Proper division plane orientation and mitotic progression together allow normal growth of maize. Proc. Natl. Acad. Sci. U. S. A. 114: 2759–2764.
Google Scholar: Author Only Title Only Author and Title

McMichael, C.M. and Bednarek, S.Y. (2013). Cytoskeletal and membrane dynamics during higher plant cytokinesis. New Phytol. 197: 1039–1057.
Google Scholar: Author Only Title Only Author and Title

Mir, R., Morris, V.H., Buschmann, H., and Rasmussen, C.G. (2018). Division Plane Orientation Defects Revealed by a Synthetic Double Mutant Phenotype. Plant Physiol. 176: 418–431.

Google Scholar: Author Only Title Only Author and Title

Müller, S., Han, S., and Smith, L.G. (2006). Two kinesins are involved in the spatial control of cytokinesis in Arabidopsis thaliana. Curr. Biol. 16: 888–894.
Google Scholar: Author Only Title Only Author and Title

Müller, S. and Jürgens, G. (2016). Plant cytokinesis-No ring, no constriction but centrifugal construction of the partitioning membrane. Semin. Cell Dev. Biol. 53: 10–18.
Google Scholar: Author Only Title Only Author and Title

Murata, T., Sano, T., Sasabe, M., Nonaka, S., Higashiyama, T., Hasezawa, S., Machida, Y., and Hasebe, M. (2013). Mechanism of microtubule array expansion in the cytokinetic phragmoplast. Nat. Commun. 4: 1967.
Google Scholar: Author Only Title Only Author and Title

Nakajima, K., Furutani, I., Tachimoto, H., Matsubara, H., and Hashimoto, T. (2004). SPIRAL1 encodes a plant-specific microtubule-localized protein required for directional control of rapidly expanding Arabidopsis cells. Plant Cell 16: 1178–1190.
Google Scholar: Author Only Title Only Author and Title

Nakaoka, Y., Miki, T., Fujioka, R., Uehara, R., Tomioka, A., Obuse, C., Kubo, M., Hiwatashi, Y., and Goshima, G. (2012). An inducible RNA interference system in Physcomitrella patens reveals a dominant role of augmin in phragmoplast microtubule generation. Plant Cell 24: 1478–1493.
Google Scholar: Author Only Title Only Author and Title

van Oostende-Triplet, C., Guillet, D., Triplet, T., Pandzic, E., Wiseman, P.W., and Geitmann, A. (2017). Vesicle Dynamics during Plant Cell Cytokinesis Reveals Distinct Developmental Phases. Plant Physiol. 174: 1544–1558.
Google Scholar: Author Only Title Only Author and Title

Pan, R., Lee, Y.-R.J., and Liu, B. (2004). Localization of two homologous Arabidopsis kinesin-related proteins in the phragmoplast. Planta 220: 156–164.
Google Scholar: Author Only Title Only Author and Title

Panteris, E. (2008). Cortical actin filaments at the division site of mitotic plant cells: a reconsideration of the "actin-depleted zone." New Phytol. 179: 334–341.
Google Scholar: Author Only Title Only Author and Title

Rasmussen, C.G. and Bellinger, M. (2018). An overview of plant division-plane orientation. New Phytol.
Google Scholar: Author Only Title Only Author and Title

Rasmussen, C.G., Sun, B., and Smith, L.G. (2011). Tangled localization at the cortical division site of plant cells occurs by several mechanisms.: 270–279.
Google Scholar: Author Only Title Only Author and Title

Sakai, T. et al. (2008). Armadillo repeat-containing kinesins and a NIMA-related kinase are required for epidermal-cell morphogenesis in Arabidopsis. Plant J. 53: 157–171.
Google Scholar: Author Only Title Only Author and Title

Sambrook, J. and Russell, D.W. (2001). Molecular Cloning: A Laboratory Manual Third. (Cold Spring Harbor Laboratory Press: Cold Spring Harbor).
Google Scholar: Author Only Title Only Author and Title

Sedbrook, J.C., Ehrhardt, D.W., Fisher, S.E., Scheible, W.-R., and Somerville, C.R. (2004). The Arabidopsis SKU6/SPIRAL1 gene encodes a plus end--localized microtubule-interacting protein involved in directional cell expansion. Plant Cell 16: 1506–1520.
Google Scholar: Author Only Title Only Author and Title

Shoji, T., Narita, N.N., Hayashi, K., Hayashi, K., Asada, J., Hamada, T., Sonobe, S., Nakajima, K., and Hashimoto, T. (2004). Plant-specific microtubule-associated protein SPIRAL2 is required for anisotropic growth in Arabidopsis. Plant Physiol. 136: 3933–3944.
Google Scholar: Author Only Title Only Author and Title

Smertenko, A. et al. (2017). Plant Cytokinesis: Terminology for Structures and Processes. Trends Cell Biol. 27: 885–894.
Google Scholar: Author Only Title Only Author and Title

Smertenko, A., Hewitt, S.L., Jacques, C.N., Kacprzyk, R., Liu, Y., Marcec, M.J., Moyo, L., Ogden, A., Oung, H.M., Schmidt, S., and Serrano-Romero, E.A. (2018). Phragmoplast microtubule dynamics - a game of zones. J. Cell Sci. 131: jcs203331.
Google Scholar: Author Only Title Only Author and Title

Suetsugu, N., Yamada, N., Kagawa, T., Yonekura, H., Uyeda, T.Q.P., Kadota, A., and Wada, M. (2010). Two kinesin-like proteins mediate actin-based chloroplast movement in Arabidopsis thaliana. Proc. Natl. Acad. Sci. U. S. A. 107: 8860–8865.
Google Scholar: Author Only Title Only Author and Title

Sugimoto, K., Williamson, R.E., and Wasteneys, G.O. (2000). New Techniques Enable Comparative Analysis of Microtubule Orientation, Wall Texture, and Growth Rate in Intact Roots of Arabidopsis. Plant Physiology 124: 1493–1506.
Google Scholar: Author Only Title Only Author and Title

Thitamadee, S., Tuchihara, K., and Hashimoto, T. (2002). Microtubule basis for left-handed helical growth in Arabidopsis. Nature 417:

193–196.
Google Scholar: Author Only Title Only Author and Title

Van Damme, D. (2009). Division plane determination during plant somatic cytokinesis. Curr. Opin. Plant Biol. 12: 745–751.
Google Scholar: Author Only Title Only Author and Title

Vanstraelen, M., Torres Acosta, J.A., De Veylder, L., Inzé, D., and Geelen, D. (2004). A plant-specific subclass of C-terminal kinesins contains a conserved a-type cyclin-dependent kinase site implicated in folding and dimerization. Plant Physiol. 135: 1417–1429.
Google Scholar: Author Only Title Only Author and Title

Völker, A., Stierhof, Y.D., and Jürgens, G. (2001). Cell cycle-independent expression of the Arabidopsis cytokinesis-specific syntaxin KNOLLE results in mistargeting to the plasma membrane and is not sufficient for cytokinesis. J. Cell Sci. 114: 3001–3012.
Google Scholar: Author Only Title Only Author and Title

Walker, K.L., Müller, S., Moss, D., Ehrhardt, D.W., and Smith, L.G. (2007). Arabidopsis TANGLED identifies the division plane throughout mitosis and cytokinesis. Curr. Biol. 17: 1827–1836.
Google Scholar: Author Only Title Only Author and Title

Wasteneys, G.O. and Collings, D.A. (2009). 3 Expanding beyond the great divide: the cytoskeleton and axial growth. Annual Plant Reviews, The Plant Cytoskeleton in Cell Differentiation and Development 10: 83.
Google Scholar: Author Only Title Only Author and Title

Wu, S.-Z., Yamada, M., Mallett, D.R., and Bezanilla, M. (2018). Cytoskeletal discoveries in the plant lineage using the moss Physcomitrella patens. Biophys. Rev.
Google Scholar: Author Only Title Only Author and Title

Yang, W., Cortijo, S., Korsbo, N., Roszak, P., Schiessl, K., Gurzadyan, A., Wightman, R., Jönsson, H., and Meyerowitz, E. (2021). Molecular mechanism of cytokinin-activated cell division in Arabidopsis. Science 371: 1350–1355.
Google Scholar: Author Only Title Only Author and Title